WIRELESS ENGINEER

Vol. XXVI OCTOBER 1949 No. 313

Radiolympia

WHILE the 16th National Radio Exhibition covers most aspects of wireless the emphasis is undoubtedly on broadcasting. The major part of the exhibits is of apparatus for use by the public and ranges from the compact so-called 'personal' portable to the large radiogramophone combined with television.

At the time of writing exhibitors have, for the most part, indicated only in outline the nature of their displays and the information available does not permit any balanced survey to be made. This must await a personal visit to Radiolympia. The indications are, however, that projection television is to be the item of most technical interest. The sets are self-contained and give a picture about 15 in by 12 in on a flat viewing screen which replaces the usual visible c.r. tube face.

The sets have obviously been designed with the object of making a larger picture available to the public than is normally practicable with direct viewing. They do not in any way displace the directly-viewed tube in the smaller sets and these are still retained for picture sizes up to 10 in by 8 in and, in some instances, for still bigger pictures.

Apart from broadcast equipment, the exhibits include business radio, v.h.f. transmitter-receivers, intercommunication sets, marine and aircraft apparatus, as well as industrial and medical apparatus. Measuring and test equipment, too, are well represented. A few firms are showing radar, but not many, for Radiolympia is not generally regarded as a radar exhibition.

As far as we can judge from the preliminary information, industrial electronics will form a very small part of the exhibition, and in this we feel that a big opportunity has been missed. The public generally, and among them we include the management and technicians of non-electronic industries, is not at all well informed about the capabilities of electronic devices. Many expect too much from them; others expect too little; and perhaps most do not realize how robust and reliable properly-designed apparatus can be.

We feel strongly that a big electronics section should have been included in Radiolympia, largely for the purpose of educating the public. As we see it, the great difficulty in establishing industrial electronics is that the industrialist is not electronically minded and when he has a job to do he thinks first of mechanical methods and last of electronic. On the other hand, the electronic engineer often does not know what jobs the industrialist wants doing.

We do not mean to imply that electronic methods are always better than the alternatives. This is far from being the case and quite often some simple mechanical gadget will perform as well as elaborate electronic gear. Each has its proper place.

This is actually being increasingly realized among the informed and there are some indications that the main place of electronics in industry will be in the combination of electronics and mechanics. Machines which are part mechanical and part electronic, each performing the part appropriate to it, may well become more widespread than either the purely mechanical or the purely electronic.

Radiolympia would have been an ideal place at which to promulgate the facts about industrial electronics. If we are right about the small part which it is to play in this year's exhibition, we hope that the opportunity will not be missed another year.

Inductance of Two Parallel Conductors

THE Editorial of October 1944 was devoted to this subject. We pointed out that in Russell's "Alternating Currents" five or six pages are devoted to a rigorous proof of the formula, and that in his "Principles of Electromagnetism" Moullin says that 'the exact solution will not be attempted.' We gave a simple proof but the following is even more direct and conclusive.

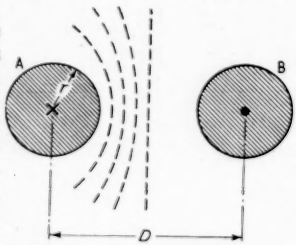

If in the figure the two conductors A and B carry equal and opposite currents the resultant magnetic field to the left of the mid-plane will link A, and that to the right of it will link B. The flux linking A, and therefore the force on A, and the e.m.f. induced in it if the current is alternating, cannot be affected in any way by an alteration in the size of B. So long as its centre remains fixed, B may be replaced by a fine filament or by a very large conductor touching the mid-plane without affecting in any way the magnetic field to the left of the mid-plane, that is, the flux linking A.

If L_a is the self-inductance per cm of A in the absence of B, that is, with a very distant return wire,

$$L_a = \int_0^r \frac{2x^3}{r^4}\,dx + \int_r^\infty \frac{2}{x}\,dx = \tfrac{1}{2} + \int_r^\infty \frac{2}{x}\,dx \text{ e.m. units}$$

the first term giving the linkages within the conductor, and the second those between its surface and infinity. If M is the mutual inductance between A and B, that is, the linkage produced in one when unit current flows in the other, it is immaterial which is regarded as the primary, and which as the secondary. In this case it is simpler to regard A as the primary and B, in the form of a fine filament, as the secondary. The flux linking the filament due to unit current in A is $\int_D^\infty \frac{2}{x}\,dx$ and this must also be the linkages produced in A by unit current in B.

The e.m.f. induced in A is therefore $I\omega L$ volts where

$$L = L_A - M = \left(\tfrac{1}{2} + \int_r^\infty \frac{2}{x}\,dx - \int_D^\infty \frac{2}{x}\,dx\right) 10^{-9}\,H$$

$$= \left(\tfrac{1}{2} + 2\log_e \frac{D}{r}\right) 10^{-9}\,H$$

and this is quite independent of the size of the other conductor. The simplicity of this proof detracts nothing from its rigorousness.

Since the flux linking either conductor due to unit current in the other one is obviously independent of the size of the latter, it follows that the mutual inductance depends only on D and is just the same whether the wires be fine filaments or massive cylindrical conductors.

The force per cm on the filament B is equal to $\frac{2I_a}{10D} \times \frac{I_b}{10}$ dynes, but this must also be the force per cm on A irrespective of its size and, since the size of B has no effect on the magnetic field in which A is situated, it cannot affect the force on it. Hence the force on A, and therefore also on B, is independent of the size of the conductors and is given by the formula $2I_aI_b/100D$ dynes per cm.

If the solid conductors be replaced by copper tubes this will not affect the mutual inductance, or the forces on the conductors, or the second term in the inductance formula; the first term in the inductance formula, which gives the linkages within the conductor, and has nothing to do with the distance between the conductors, will of course, be modified.

The assumption has been made throughout that the current is uniformly distributed over the cross-section of the conductors, or is, at least, symmetrical about the centres. If the frequency is so high that there is an appreciable departure from symmetry, the effective distance between the conductors will be modified.

G. W. O. H.

WAVEGUIDE FIELD PATTERNS IN EVANESCENT MODES

By A. L. Cullen, B.Sc., A.M.I.E.E.

SUMMARY.—Field patterns in a waveguide at frequencies below cut-off are calculated, both for a single evanescent field, and for two oppositely attenuated ('incident' and 'reflected') fields. Isometric projection of the surface depicting the electric field in the guide is found to provide a useful picture of the field distribution.

1. Introduction

THE evanescent electromagnetic field, in a waveguide operated below its cut-off frequency, is important in practice because its amplitude falls off exponentially with distance along the guide at an accurately calculable rate, and so may be used as a reference standard of attenuation. Attenuators employing this principle are generally known as 'piston attenuators,' and were in common use at a time when propagating waveguides were little more than a scientific curiosity. Waveguide theory is, however, well adapted to calculations of the performance of piston attenuators, and has been employed in most recent contributions to the subject.

Although the field patterns of propagating modes in waveguides have received considerable attention, and isometric diagrams representing the field distribution have been prepared,[1,2] no similar study of evanescent modes appears to have been made. In the belief that these isometric patterns provide a useful visual aid to the formation of a mental picture of the field, such a study is undertaken in the present paper.

2. Field Pattern of Evanescent Modes

Using a rectangular co-ordinate system as shown in Fig. 1, the field components for an evanescent H_{01} mode in a rectangular waveguide are :—

$$\left.\begin{aligned} H_x &= \cos\left(\frac{\pi z}{b}\right) e^{-\alpha x} \sin \omega t \\ H_z &= \frac{\alpha b}{\pi} \sin\left(\frac{\pi z}{b}\right) e^{-\alpha x} \sin \omega t \\ \mathscr{E}_y &= \frac{\omega \mu b}{\pi} \sin\left(\frac{\pi z}{b}\right) e^{-\alpha x} \cos \omega t \end{aligned}\right\} \quad \ldots \quad (1)$$

where $$\alpha = \frac{\pi}{b}\sqrt{1 - \left(\frac{2b}{\lambda}\right)^2} \quad \ldots \quad \ldots \quad (2)$$

The electric and magnetic fields exhibit no variation of phase with position, and at all points the electric field is in quadrature with the magnetic field. The time average Poynting vector is therefore zero and there is no power flow.

The distribution of the electric field is readily visualised. The electric lines of force are everywhere parallel to the y-axis and the transverse distribution of electric field strength is of precisely the same sinusoidal form as in the familiar case of a propagating guide. Along the guide, however, the field strength decreases exponentially with distance from the source, at a rate determined by the critical dimensions of the guide and the free-space wavelength.

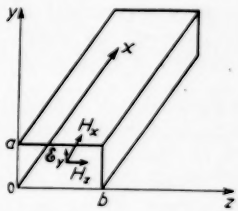

Fig. 1. *Co-ordinate system.*

To calculate the form of the magnetic-field lines in an x, z plane, we observe that the slope of such a line at any point is given by the ratio of the corresponding magnetic-field components at that point. Thus, referring to Fig. 2, and equation (1), we have, at any point :—

$$\frac{dx}{dz} = \frac{H_x}{H_z} = \frac{\pi}{\alpha b} \cot\left(\frac{\pi z}{b}\right) \quad \ldots \quad \ldots \quad \ldots \quad (3)$$

Integrating this expression leads to the result :

$$\begin{aligned} x - x_0 &= \frac{1}{\alpha} \log_e \sin\left(\frac{\pi z}{b}\right) \\ &= -\frac{1}{\alpha} \log_e \operatorname{cosec}\left(\frac{\pi z}{b}\right) \quad \ldots \quad \ldots \quad (4) \end{aligned}$$

in which x_0 is an arbitrary constant of integration. It will be seen that all the field lines have the same form, the different lines obtained by giving different values to x_0 being identical if referred to x_0 as origin. It will also be noted that the effect of a variation in frequency is to stretch or compress the scale of the x-axis in accordance with the variation in the attenuation coefficient α. If the operating frequency is well below the cut-off frequency of the guide, so that $\lambda \gg 2b$, α is nearly equal to π/b nepers per unit length of guide as will be seen from equation (2), and is practically independent of frequency. This is the

MS accepted by the Editor, November 1948

normal operating condition of a piston attenuator, for the attenuation is then nearly independent of frequency. Magnetic lines of force for this case are plotted in Fig. 3. The attenuation in a length of guide equal to b is π nepers or 27.3 db. Thus an attenuation of 6 db takes place in 0.220 b. The lines of force in Fig. 3 are drawn at 6-db intervals.

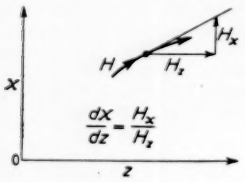

Fig. 2. *Calculation of slope of lines of force.*

The current streamlines are everywhere perpendicular to the magnetic lines of force, and form an orthogonal family of curves. These curves are given by replacing $\frac{dx}{dz}$ by $-\frac{dz}{dx}$ in equation (3) and integrating. Taking $\alpha = \pi/b$ as before, we find :

$$x - x_0 = -\frac{1}{\alpha}\log_e \sec\left(\frac{\pi z}{b}\right) \quad .. \quad .. \quad (5)$$

in which x_0 again represents a constant of integration. The current streamlines given by equation (5) are also plotted in Fig.3 as full lines.

An instructive three-dimensional representation of the electromagnetic field in an evanescent mode may be obtained in the following way. Consider the representation of $\mathcal{E}_y$ as a surface defined by

$$\mathcal{E}_y = e^{-\alpha x}\sin\left(\frac{\pi z}{b}\right)\cos \omega t \quad .. \quad .. \quad (6)$$

in which $\mathcal{E}_y$ has unit amplitude at the point $x = 0, z = b/2$.

This surface is plotted in an isometric projection in Fig. 4, for the case $\alpha = \pi/b$, at $\omega t = 0$.

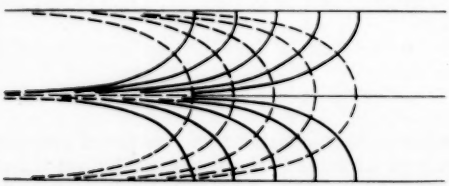

Fig. 3. *Magnetic lines of force in evanescent mode.*

Any transverse section is sinusoidal, and any longitudinal section is exponential. In the first place, at any point x, z, the ordinate is equal to the electric field strength $\mathcal{E}_y$. Thus the surface gives a representation of the distribution of electric field in the guide. The transverse-magnetic field, H_z has the same distribution, and its intensity may also be represented by this surface. Next, consider the curves defined by the intersection of the surface by horizontal planes, and shown as dotted lines in Fig. 4. These curves are given by putting $\mathcal{E}_y$ = const. in equation (6). If the constant is written $e^{-\alpha x_0}$, (6) reduces directly to equation (4), and so we find that the curves considered are in fact identical with the magnetic lines of force plotted in Fig. 3. The magnetic field strength *along* a line of force is given by $H = \sqrt{H_x^2 + H_z^2}$ and using equation (1), it is easy to see that when $\alpha = \pi/b$ we have :—

$$H = e^{-\alpha z}\sin \omega t \quad .. \quad .. \quad .. \quad (7)$$

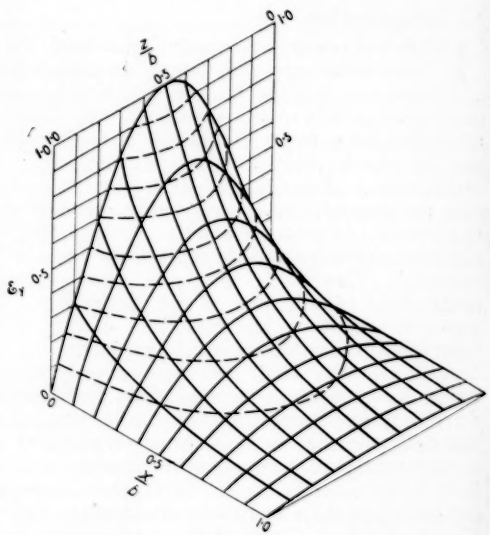

Fig. 4. *The surface* $\mathcal{E}_y = \frac{-\pi x}{b}\sin\left(\frac{\pi z}{b}\right)$ *representing* $\mathcal{E}_y$ *at* $\omega t = 0$ *and* H *at* $\omega t = \pi/4$. *---- magnetic lines of force.*

It is interesting to notice that this resultant magnetic field is independent of z.

To get a complete picture of the electric field, imagine that the whole surface is vibrating sinusoidally in a vertical direction, assuming equal positive and negative limiting values on successive half cycles, so that the surface appears first as a hill, as in Fig. 4, then flattens off to a plain, dips down to a valley, the complement of the previous hill, then back to a plain, and so on.

The magnetic field intensity also vibrates sinusoidally in time, but is always lagging by $\pi/2$ behind the electric field.

3. Mechanism of Power Flow

It has already been pointed out that the electromagnetic field in an evanescent mode decays exponentially with distance along the guide, and that the action of a piston attenuator is based

upon this principle. This raises a paradox, however, for we have seen that the power flow in a single evanescent mode is zero, whereas we know that in fact power does flow from input to output in a piston attenuator. In general, however, we would expect to have a second evanescent mode set up by 'reflection' at the output coupling device, decaying exponentially in the opposite direction along the guide. This field is analogous to the reflected wave on a mismatched transmission line. As Huxley[3] has shown, it is only in the presence of such a 'reflected' field that power can be transported by a waveguide operated below the cut-off frequency. Although either field alone cannot carry power, the two together carry an amount of power depending on their amplitudes, and on the phase angle between them. (Note that in an evanescent mode, there is no change of phase with distance along the guide).

To calculate the power flow, we must find the Poynting vector for the resultant *field*, for it is the field components, and not the powers, which

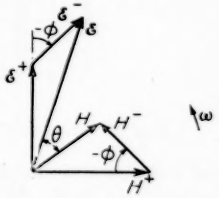

Fig. 5. *Time-vector diagram of resultant field.*

may be superimposed. If the 'incident' electromagnetic field, (with a factor $e^{-\alpha x}$) is denoted by $\mathscr{E}^+$, H^+ and the 'reflected' field by $\mathscr{E}^-$, H^-, the resultant field $\mathscr{E}$, H, will be as shown in the time-vector diagram of Fig. 5. It will be seen that the resultant $\mathscr{E}$ and H are not in quadrature, but differ in phase by an angle θ, less than $\pi/2$ if the source is to the 'left' (i.e., on the negative side of the x-axis.) Thus a power flow $\mathscr{E}H\cos\theta$ exists, and its magnitude is clearly dependent on the precise value of ϕ, the phase angle between the incident and the reflected fields.

The nature of this dependence may be evaluated as follows. The power flow P in the positive x-direction, is given by $\mathscr{E}H\cos\theta$ or alternatively, using complex vector notation by :

$$P = \text{Re}\ (\mathscr{E}^+ + \mathscr{E}^-)\ (H_*^+ + H_*^-) \quad .. \quad (8)$$

where $H_*^{\pm}$ is the conjugate complex of $H^{\pm}$. Expanding (8), we have :—

$$P = \text{Re}\ (\mathscr{E}^+ H_*^+ + \mathscr{E}^- H_*^- + \mathscr{E}^+ H_*^- + \mathscr{E}^- H_*^+)$$

The first two terms of this expression give the power transported by the incident and reflected waves respectively in the absence of the other, and so these terms are, as we have already seen, both zero. If we introduce a reflection coefficient $\rho = |\rho| e^{j\phi} = \dfrac{\mathscr{E}^-}{\mathscr{E}^+} = -\dfrac{H^-}{H^+}$ and denote the reactive characteristic impedance by $jX_0 = \dfrac{\mathscr{E}^+}{H^+} = -\dfrac{\mathscr{E}^-}{H^-}$ we find :

$$P = \text{Re}\ [-jX_0 H^+ |\rho| e^{-j\phi} H_*^+ + jX_0 H^+ |\rho| e^{j\phi} H_*^+]$$

$$= \text{Re}\ [-je^{j\phi} + je^{+j\phi}]\ |\rho|\ X_0 H^+ H_*^+$$

$$\text{or } P = -2|\rho|\ X_0 H^+ H_*^+ \sin\phi \quad .. \quad (9)$$

It follows that P is greatest, for given values of H^+, X_0 and $|\rho|$, when $\phi = -\pi/2$. This result is suggested by inspection of the vector diagram, for it makes $\mathscr{E}^-$ in phase with H^+, and $\mathscr{E}^+$ in phase with H^-. It represents optimum operating conditions for a piston attenuator, in the sense that it gives the minimum possible standing loss for a given permissible departure from a linear decibel attenuation law.

To understand the reason for this, it is necessary to observe that the whole of the power supplied to the attenuator is delivered to the output, neglecting conductor losses. The piston attenuator attenuates by mismatching, its input impedance being highly reactive for large attenuations, and developing an increasing resistive component, corresponding to power delivered at the output, as the amount of attenuation is decreased.

The power developed by the source is thus mainly dissipated in its own internal resistance, the whole of the amount accepted by the attenuator being delivered to the load, if conductor losses are negligible.

Thus, by the very nature of the operation of such attenuators, there is necessarily a variation of input impedance when the attenuation is altered. It is only when the variation of input impedance is negligible that a linear decibel scale of attenuation is obtained.

The variation of input impedance depends on the relative amplitudes of the reflected and incident fields, and may be made as small as desired by increasing the minimum attenuation setting. A stop may be fixed on the attenuator to prevent movement of the output coupling beyond this limit, set by the required degree of linearity. It is clear that the 'standing loss' is determined by this procedure, and that a compromise between linearity and standing loss is inevitable. Nevertheless, as we have seen, for given amplitudes of incident and reflected fields, the power delivered is a maximum, and hence the standing loss a minimum, when the phase angle between them is 90°, and this clearly corresponds to optimum design for the present purpose.

In what follows, we shall restrict our discussion to the case $\phi = -\pi/2$, so that the reflected electric field *lags* by $\pi/2$ on the incident electric

field. We have assumed in (1) that $\mathcal{E}_y$ varies with time in accordance with the factor $\cos \omega t$, and if this is taken to be the incident field, it follows that the reflected electric field will vary with time as $\sin \omega t$.

4. Field Pattern in Waveguide Attenuator

We have seen that the essence of operation of a piston attenuator is the presence of a reflected evanescent field. In this section we shall investigate the resultant field pattern in a waveguide operating under these conditions. The incident field we take to be that given by (1), and the reflected field, reversing the sign of H_2 relative to $\mathcal{E}_y$ and changing the time-factors to give the required phase difference of $-\pi/2$ in the fields, we find :—

$$\left.\begin{aligned} H_x^- &= -\cos\left(\frac{\pi z}{b}\right) e^{\alpha(x-l)} \cos \omega t \\ H_z^- &= \frac{\alpha b}{\pi} \sin\left(\frac{\pi z}{b}\right) e^{\alpha(x-l)} \cos \omega t \\ \mathcal{E}_y^- &= \frac{\omega \mu b}{\pi} \sin\left(\frac{\pi z}{b}\right) e^{\alpha(x-l)} \sin \omega t \end{aligned}\right\} \quad .. \quad (10)$$

The arbitrary amplitude of $\mathcal{E}_y^-$ relative to $\mathcal{E}_y^+$ is taken into account by l which may be regarded as an arbitrary constant. $\mathcal{E}_y^+ = \mathcal{E}_y^-$ when $x = l$. As before, we introduce a surface representing the electric field intensity as a function of x and z.

This is clearly given by :—

$$\mathcal{E}_y = \sin\left(\frac{\pi z}{b}\right) e^{-\alpha x} \cos \omega t + \sin\left(\frac{\pi z}{b}\right) e^{\alpha(x-l)} \sin \omega t \quad .. \quad .. \quad .. \quad (11)$$

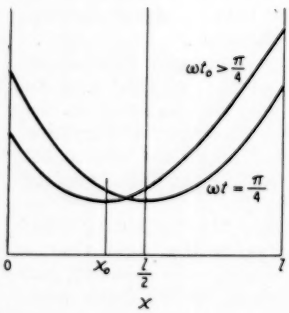

Fig. 6. *Illustrating movement of field pattern.*

Now this surface, we see at once, varies in *shape* with time, unlike the surface defined by equation (6) for a single evanescent field, into which time entered only as a scaling factor.

However, we shall soon see that the situation may be reduced to three principal cases :—

(i) $\sin \omega t = 0$ or $\cos \omega t = 0$.

(ii) $\cos \omega t$ and $\sin \omega t$ of the same sign.

(iii) $\cos \omega t$ and $\sin \omega t$ of opposite sign.

Take case (i) first. If $\sin \omega t = 0$, $\cos \omega t = 1$, and the electromagnetic field distribution may be built up from the previous calculations. The electric field is simply that due to the incident field, the electric part of the reflected field being zero. The distribution of electric field at this instant, say $\omega t = 0$, is precisely that corresponding to the $\mathcal{E}_y$ surface of Fig. 4. The magnetic part of the incident field is, however, zero at $\omega t = 0$,

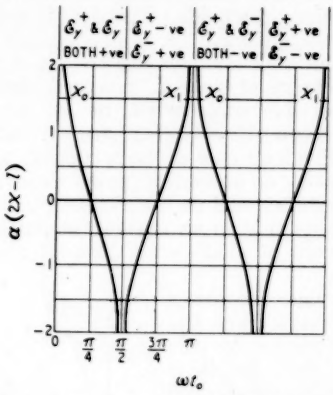

Fig. 7. *Movement of resultant field pattern.*

and the magnetic field at this time is that due to the reflected field. It will follow lines of force of precisely the same character as those of Figs. 3 and 4, but directed towards the negative direction of x. If $\cos \omega t = 0$, $\sin \omega t = 1$ and the field pattern is similar to that described above, but oppositely directed in space.

Now consider case (ii). First note that when $x = l/2$ the incident and reflected components are equal when $\omega t = \pi/4$.

Equation (11) then becomes :—

$$\mathcal{E}_y = \sqrt{2}\, e^{-\alpha l/2} \sin\left(\frac{\pi z}{b}\right) \cosh \alpha\,(x - l/2) \quad (12)$$

so that the variation of $\mathcal{E}_y$ with x has the form of a cosh curve centred on $x = l/2$. At a slightly later instant, t_0, the reflected field will be greater than the incident field at $x = l/2$ as will be clear from equation (11), but at a suitably chosen smaller value of x say x_0, the fields are again equal, and the electric field distribution follows a cosh curve with respect to x at the instant t_0 this time centred on x_0. A value of x_0 which satisfies this condition at time t_0 can always be found provided that $\cos \omega t_0$ and $\sin \omega t_0$ are both positive, or both negative, the field in the latter case having the opposite instantaneous direction. This is illustrated in Fig. 6. The criterion is :

$$e^{-\alpha x_0} \cos \omega t_0 = e^{\alpha(x_0 - l)} \sin \omega t_0$$

and this leads to :—

$$e^{\alpha(2x_0 - l)} = \cot \omega t_0$$

$$\text{or } 2x_0 - l = -\frac{1}{\alpha}\log_e \cot \omega t_0 \quad .. \quad .. \quad (13)$$

This equation has physical significance when $\cot \omega t_0 > 0$. In Fig. 7 $\alpha(2x_0 - l)$ is plotted as a function of ωt_0.

In case (iii), note that at $x = l/2$ the incident and reflected components are equal and opposite when $\omega t = -\pi/4$.

Equation (11) then gives :—

$$\mathcal{E}_y = -\sqrt{2}\, e^{-la/2} \sin\left(\frac{\pi z}{b}\right) \sinh \alpha(x - l/2) \quad (14)$$

The variation of $\mathcal{E}_y$ with x has therefore the form of a sinh curve centred on $x = l/2$, and as before we find that at any other instant of time t_0 for which the signs of $\cos \omega t$ and $\sin \omega t$ differ, a point x_1 can be found at which the incident and

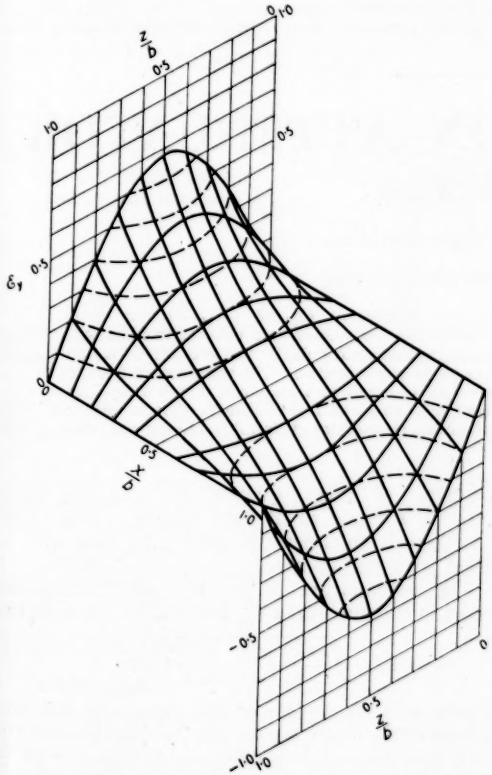

Fig. 8. $\mathcal{E}_y$ *at* $\omega t = -\pi/4$. ---- *magnetic field at* $\omega t = -\pi/4$.

reflected fields are equal and opposite, and about which the $\mathcal{E}_y$ — surface has a sinh-variation with x. We find :—

$$2x_1 - l = \frac{1}{\alpha}\log_e(-\cot \omega t_0) \quad .. \quad .. \quad (15)$$

and values of x_1 as a function of ωt_0 are also plotted in Fig. 7.

The equation has meaning only when $\cot \omega t_0$ is negative.

Thus it is sufficient to consider the instants $\omega t = -\pi/4$, $\omega t = 0$, and $\omega t = +\pi/4$ to visualize all possible forms the field can take. The distribution at any other instant can be derived from these curves by shifting the origin of x and adjusting the vertical scale.

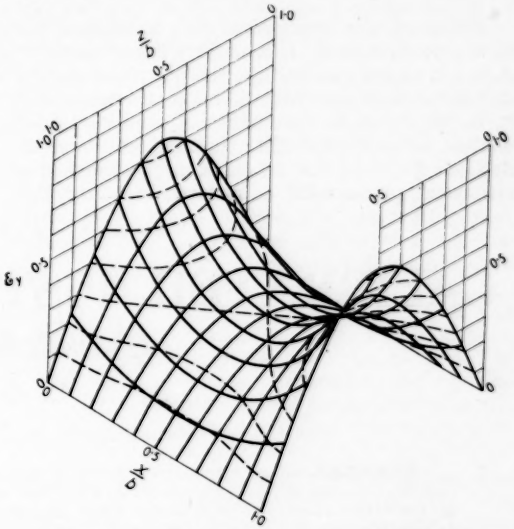

Fig. 9. $\mathcal{E}_y$ *at* $\omega t = +\pi/4$. ---- *magnetic field at* $\omega t = +3\pi/4$.

The $\mathcal{E}_y$-surface is therefore plotted for $\omega t = -\pi/4$ in Fig. 8, and for $\omega t = +\pi/4$ in Fig. 9. The case $\omega t = 0$ is covered by the case of a single evanescent mode dealt with in Section 2.

We now turn to a consideration of the magnetic field.

Combining equations (1) and (10) we get :—

$$H_x = \cos\left(\frac{\pi z}{b}\right)\left[e^{-\alpha x}\sin \omega t - e^{\alpha(x-l)}\cos \omega t\right]$$

$$H_z = \frac{\alpha b}{\pi}\sin\left(\frac{\pi z}{b}\right)\left[e^{-\alpha x}\sin \omega t + e^{\alpha(x-l)}\cos \omega t\right]$$

and so the field lines are defined by the following differential equation :

$$\frac{dx}{dz} = \frac{H_x}{H_z} = \frac{\pi}{\alpha b}\cot\left(\frac{\pi z}{b}\right)\left[\frac{e^{-\alpha x}\sin \omega t - e^{\alpha(x-l)}\cos \omega t}{e^{-\alpha x}\sin \omega t + e^{\alpha(x-l)}\cos \omega t}\right]$$

$$\text{or } \frac{1}{\alpha}\log_e \sin\left(\frac{\pi z}{b}\right) = \frac{1}{\alpha}\int \frac{e^{-\alpha x}\sin \omega t + e^{\alpha(x-l)}\cos \omega t}{e^{-\alpha x}\sin \omega t - e^{\alpha(x-l)}\cos \omega t}\, d(\alpha x)$$

Note that the numerator of the integral is minus the differential with respect to αx of the denominator, so we get :—

$$-\log_e \sin\left(\frac{\pi x}{b}\right) = \log_e [e^{-ax} \sin \omega t - e^{a(x-b)} \cos \omega t] - \log_e A$$

where A is an arbitrary constant.

Finally, therefore, we have :—

$$A \operatorname{cosec}\left(\frac{\pi z}{b}\right) = e^{-ax} \sin \omega t - e^{a(x-b)} \cos \omega t \quad (16)$$

Comparing this expression with equation (11), we see at once that if ωt in (11) is replaced by $\omega t - \pi/2$ to take account of the 90° phase difference between the electric and magnetic fields, and $\mathscr{E}_y$ is put equal to a constant A, equation (16) results. Thus we find that the magnetic lines of force are given by the curves of inter-section of a horizontal plane with a surface depicting the electric field distribution a quarter-cycle earlier. Thus the magnetic lines of force corresponding to $\omega t = \pi/4$ have been superimposed on the $\mathscr{E}_y$ surface corresponding to $\omega t = -\pi/4$, and the magnetic lines of force corresponding to $\omega t = 3\pi/4$ have been superimposed on the $\mathscr{E}_y$ surface corresponding to $\omega t = \pi/4$. (See Figs. 8 and 9).

It is helpful in visualizing Fig. 8 as a 'three-dimensional' figure to view it also upside down.

5. Acknowledgment

The author wishes to acknowledge the encouragement he has received from Professor H. M. Barlow.

REFERENCES

[1] L. J. Chu & W. L. Barrow. *Proc. Inst. Radio Engrs*, Vol. 26, 1938, pp. 1520–1555.

[2] H. H. Skilling "Fundamentals of Electric Waves" Wiley, p. 164.

[3] L. G. H. Huxley, "Wave Guides," Cambridge University Press, p. 62.

CALIBRATED PISTON ATTENUATOR

For Millimetre Waves

By A. C. Gordon-Smith

(Communication from the National Physical Laboratory)

SUMMARY.—The attenuator, which operates in the evansecent H_{11} or TE_{11} circular mode, consists of a pair of telescoping brass tubes. The outer tube has a diameter such that when filled with air the attenuation is about 7 db per mm. The inner tube is filled with polystyrene and acts as a non-attenuating waveguide for the H_{11} mode but does not transmit other modes. The attenuation per mm of movement has been measured, after frequency conversion, in terms of a standard piston attenuator and agreement obtained between the measured and theoretical values within the limits of experimental accuracy. It has also been confirmed that the crystal mixer and its associated circuit is a linear converter at a wavelength of 6 mm.

1. Introduction

IN measurement work at wavelengths near to 6 mm the need has arisen for an accurate variable attenuator. At longer wavelengths the piston attenuator described by Harnett and Case[1] and by George[2] is now a familiar laboratory instrument, and the present work describes the results of a successful attempt to apply a similar technique to millimetre wavelengths.

2. Description of the Instrument

A drawing of the piston attenuator is given in Fig. 1. It is designed to operate at wavelengths near to 6 mm and is excited in the H_{11} or TE_{11} circular evanescent mode. The use of the dominant mode has the obvious advantage that other unwanted modes are more rapidly attenuated. The instrument consists of a pair of telescoping brass tubes of circular cross-section. The outer tube A has been accurately reamed to have a diameter of 2.820 ±0.012 mm and the inner tube B is made to fit very closely. The latter has a wall thickness of only 0.13 mm and is filled with polystyrene.

The attenuation of an H_{11} electromagnetic wave in the air-filled tube is given by the formula

$$\alpha = 8.69\sqrt{\left(\frac{1.841}{a}\right)^2 - \left(\frac{2\pi}{\lambda}\right)^2} \text{ db/cm}$$

where a is the radius of the tube and λ is the wavelength in free space. In this case $a = 0.1410 \pm 0.0006$ cm and $\lambda = 0.622$ cm so that $\alpha = 72 \pm 1$ db/cm.

The polystyrene, which fills the inner tube, has[3] a dielectric constant of 2.55. This increases the critical wavelength and transforms the tube into a non-attenuating waveguide for the H_{11} mode at wavelengths below 6.9 mm. The critical wavelength for this mode is given by $\lambda_c = 1.71\, d\sqrt{K}$, where d is the diameter and K is the

dielectric constant. Other modes are not propagated in this tube because the critical wavelength for the next possible mode (i.e., the E_{01}) is 5.3 mm, given by the relation $\lambda_c = 1.31\, d\sqrt{K}$.

The attenuator is fed from a coupling hole in the broad side of a piece of rectangular guide G of internal cross-sectional dimensions 4.8 × 2.4 mm, which is terminated by an adjustable piston P. The diameter of the coupling hole is the same size as the internal diameter of the attenuating tube A. The output from tube B is coupled in the same manner to another length of similar rectangular guide H. Adjustment of the attenuator is made by means of a micrometer head M, which can be read to 0.001 mm, and a compressed spring S supplies the restoring force. A piece of rectangular guide about 1 ft (0.3 m) long is added to the guide G and is sufficiently flexible to allow the necessary axial movement of the cylinder. Guide rods R are fitted to prevent any rotational movement.

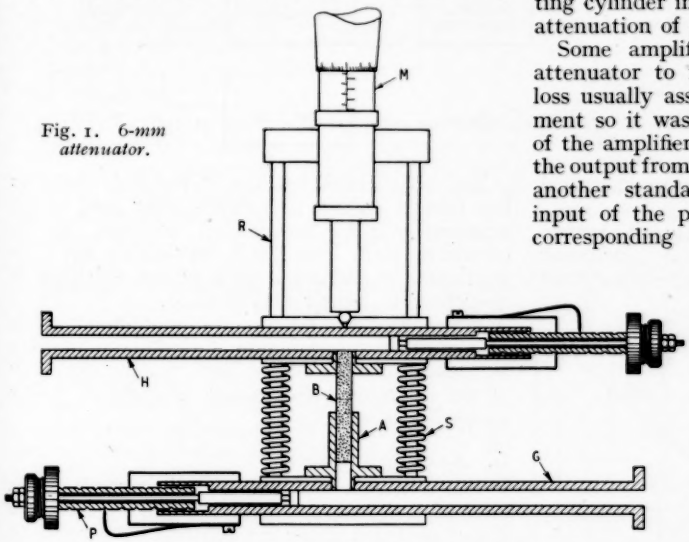

Fig. 1. *6-mm attenuator.*

3. Calibration

A schematic diagram of the circuit used for the calibration of the attenuator is given in Fig. 2. Power at a wavelength of 6.22 mm was produced from a klystron, operating at 12.44 mm, by means of a crystal distorter. The second-harmonic power was fed to the piston attenuator through a rectangular guide suitable for propagating power at a wavelength of 6.22 mm but with a cut-off wavelength far below that of the fundamental. Matching stubs were incorporated at the input and at the output of the attenuator. The output power from the attenuator was applied to a crystal mixer. Another klystron, operating at 12.5 mm, was used as a local oscillator to produce an intermediate-frequency output at 30 Mc/s. This was amplified by means of a wide-band amplifier, having a bandwidth of 2 Mc/s for a 1-db reduction in output voltage.

An intermediate-frequency piston attenuator of known characteristics was incorporated in the amplifier. The internal diameter of the attenuating cylinder in this case was 6.35 cm giving an attenuation of 5.04 db/cm over the linear range.

Some amplification was needed before this attenuator to make up for the large insertion loss usually associated with this type of instrument so it was necessary to check the linearity of the amplifier used. This was done by feeding the output from a 30-Mc/s signal generator through another standard piston attenuator on to the input of the pre-amplifier and confirming that corresponding changes of attenuation on the two attenuators did agree when a fixed output was maintained from the final stage. This was found to be the case over a range of about 60 db and so in the final calibration the input to the 6-mm attenuator was adjusted so that this range only was used.

In order to improve the signal-to-noise ratio of the receiver, the source was modulated at 1,000 c/s and a rectifier, together with a selective 1,000-c/s amplifier, was added to the intermediate-frequency amplifier. The bandwidth of the audio amplifier was 50 c/s for a 6-db reduction of output voltage. Finally the audio output was rectified by means of a crystal and the resulting direct current measured on a microammeter.

The 6-mm attenuator was then calibrated in terms of the 30-Mc/s attenuator. The matching stubs were readjusted before each observation over the first 3 mm of attenuation but after this, rematching was found to be unnecessary.

Although the klystron oscillators were operated from stabilized supplies and a period of about three hours was allowed in order to reach steady temperature conditions, it was found that the local oscillator needed to be retuned occasionally during the experiment.

The results obtained are given in Fig. 3. It will be seen that after the first 3.5 mm of attenuation, corresponding to 10 db, the graph is a straight line and the slope gives the measured attenuation of 7.1 db per mm. This confirms that the crystal mixer and its associated circuit

is an accurately-linear converter when operating at wavelengths near to 6 mm, if one excludes the unlikely possibility that the mixer and the 6-mm attenuator have exactly compensating laws.

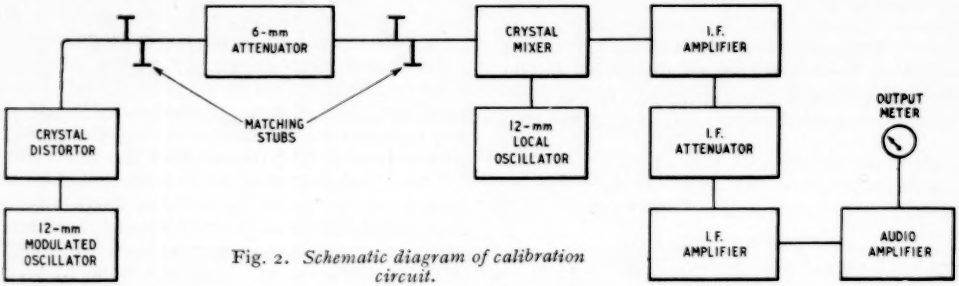

Fig. 2. *Schematic diagram of calibration circuit.*

The rectified crystal current due to the local oscillator was about 1 mA.

A separate experiment was carried out to determine the insertion loss of the instrument and it was found to be less than 1 db with correct matching conditions.

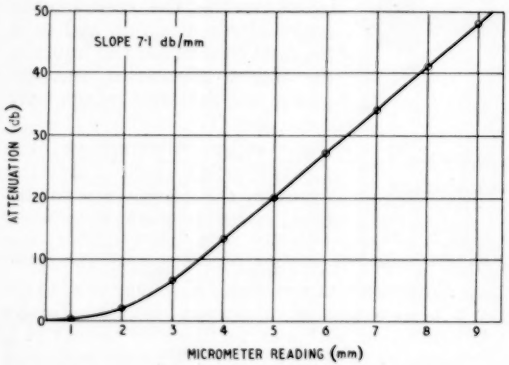

Fig. 3. *Calibration of 6-mm attenuator.*

4. Conclusions

The measured attenuation of the instrument of 7.1 db per mm of piston movement agrees within experimental accuracy with the value of 7.2 ± 0.1 per mm calculated from the measured values of the diameter and the wavelength.

The actual insertion loss of the instrument is less than 1 db but if the non-linear part of the attenuator is to be avoided the first 10 db cannot be used. This loss is appreciably less than that usually obtained with piston attenuators operating at longer wavelengths.

When improved sources of power are available at a wavelength of 6 mm it should be possible to make fuller use of the high reading accuracy of the instrument to measure changes in power as small as 0.01 db.

5. Acknowledgments

The work described above was carried out as part of the programme of the Radio Research Board and this paper is published by permission of the Department of Scientific and Industrial Research. The author desires to acknowledge the advice given by Dr. J. A. Saxton and the assistance of M. W. Barker who made the instrument.

REFERENCES

[1] D. E. Harnett and N. P. Case, "The Design and Testing of Multirange Receivers," *Proc. Inst. Radio Engrs*, 1935, Vol. 23, p. 578.

[2] R. W. George, "Field Strength Measuring Equipment for Wide-Band Ultra-High-Frequency Transmission," *R.C.A. Review*, 1939, Vol. 3, p. 431.

[3] R. P. Penrose, "Some Measurements of the Permittivity and Power Factor of Low-Loss Solids at 25,000 Mc/s Frequency," *Trans. Far. Soc.*, 1946, Vol. 42A, p. 108.

ASYMMETRICAL MULTIVIBRATORS

By R. Feinberg, Dr. Ing., M.Sc.

(Electrical Engineering Dept., University of Manchester)

SUMMARY.—It is shown that the frequency and the waveform of oscillation of an asymmetrical multivibrator with pentodes can be computed with the help of simple formulæ provided the circuit is so designed that one of the two anode voltages is of rectangular or near-rectangular shape when the multivibrator is in the steady state of operation. The waveform of the other anode voltage may be rectangular or triangular and may be varied within a fairly wide range without interfering with the frequency of oscillation. The frequency of oscillation may be altered without disturbing the waveform by changing the capacitance values but keeping their ratio constant. Predicted frequencies and waveforms are verified by experiment.

Introduction

THE oscillation produced by a multivibrator circuit with pentodes was analysed in a previous paper[1] for the case of a symmetrical circuit arrangement. It is the purpose of this paper to present an analysis of the asymmetrical case of a multivibrator circuit with pentodes.

The line of approach to solving the problem and the mathematical methods used are similar to the investigation of the symmetrical case. As in the symmetrical case the assumptions on which the analysis rests are: (1) the pentodes operate on the coalescent parts of their characteristics, (2) the circuit performance is independent of the inter-electrode valve capacitances and of the self-capacitances and self-inductances of the circuit elements.

The analysis is limited to the practically important case that the two pentodes have identical characteristics.

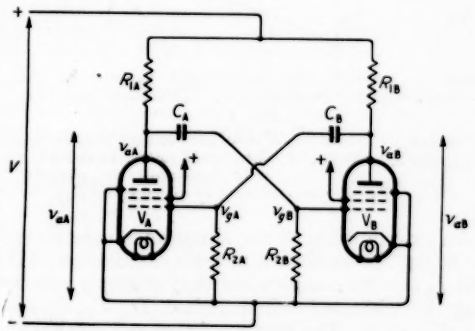

Fig. 1. *Circuit diagram of the asymmetrical multivibrator with pentodes.*

Multivibrator Oscillation

Fig. 1 shows the asymmetrical multivibrator circuit with pentodes and Fig. 2 gives the associated equivalent diagram. The resistances r_g represent the resistance of control grid to cathode of a valve at a positive control-grid voltage, and r_a is the anode slope resistance of a pentode at the coalescent part of its characteristic.

MS accepted by the Editor, January 1949

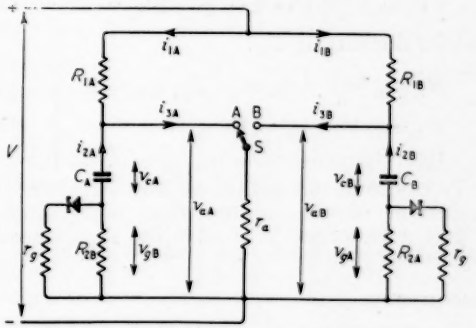

Fig. 2. *Equivalent diagram of the asymmetrical multivibrator circuit with pentodes.*

Fig. 3 gives a typical example of the waveforms of anode and control-grid voltages produced with an asymmetrical multivibrator of the type of Fig. 1. T_A is the period of time when valve V_A is conducting and V_B non-conducting (i.e., C_A discharging and C_B charging), and T_B is the part-period when V_B is conducting and V_A non-conducting (and hence C_B discharging and C_A charging).

Let T_{cA} and T_{cB}, respectively, be the time-constants of charging C_A and C_B and let T_{dA} and T_{dB}, respectively, be the time-constants of discharging C_A and C_B. The shape of the anode voltage v_{aA} in the part-period T_B is determined by the ratio T_{cA}/T_{dB} and the shape of v_{aB} during T_A by the ratio T_{cB}/T_{dA}. The voltage shape is rectangular when the respective time-constant ratio is $\ll 1$, and the voltage shape is triangular when the ratio is $\gg 1$.

Equations

The multivibrator equations are based on the equivalent diagram of Fig. 2. Switch S in

position A means that valve V_A is conducting and V_B non-conducting. In this position C_A is discharging and C_B charging. We have the following equations for discharging C_A:

$$\left.\begin{aligned} R_{1A}\, i_{1A} - \frac{1}{C_A}\int i_{2A}\, dt - R_{2B}\, i_{2A} &= V \\ R_{1A}\, i_{1A} + r_a\, i_{3A} &= V \\ i_{1A} + i_{2A} - i_{3A} &= 0 \end{aligned}\right\} \quad (1)$$

and for charging C_B:

$$R_{1B}\, i_{1B} + \frac{1}{C_B}\int i_{1B}\, dt + \frac{R_{2A}\, r_g}{R_{2A} + r_g}\, i_{1B} = V \quad (2)$$

When switch S is in position B, V_B is conducting and V_A non-conducting, and C_B is discharging and C_A charging. The equations are for charging C_A:

$$R_{1A}\, i_{1A} + \frac{1}{C_A}\int i_{1A}\, dt + \frac{R_{2B}\, r_g}{R_{2B} + r_g}\, i_{1A} = V \quad (3)$$

and for discharging C_B:

$$\left.\begin{aligned} R_{1B}\, i_{1B} - \frac{1}{C_B}\int i_{2B}\, dt - R_{2A}\, i_{2B} &= V \\ R_{1B}\, i_{1B} + r_a\, i_{3B} &= V \\ i_{1B} + i_{2B} - i_{3B} &= 0 \end{aligned}\right\} \quad (4)$$

To calculate the frequency and waveform of oscillation of the asymmetrical multivibrator circuit it is necessary to solve the simultaneous equations (1) to (4).

Frequency

The time-constant T_{cA} for charging C_A is

$$T_{cA} = C_A\left(R_{1A} + \frac{R_{2B}\, r_g}{R_{2B} + r_g}\right) \quad .. \quad .. \quad (5)$$

and the time-constant T_{dA} for discharging C_A

$$T_{dA} = C_A\left(R_{2B} + \frac{R_{1A}\, r_a}{R_{1A} + r_a}\right) \quad .. \quad .. \quad (6)$$

The time-constant T_{cB} for charging C_B is

$$T_{cB} = C_B\left(R_{1B} + \frac{R_{2A}\, r_g}{R_{2A} + r_g}\right) \quad .. \quad .. \quad (7)$$

and the time-constant T_{dB} for discharging C_B

$$T_{dB} = C_B\left(R_{2A} + \frac{R_{1B}\, r_a}{R_{1B} + r_a}\right) \quad .. \quad .. \quad (8)$$

The period T of multivibrator oscillation becomes with the notation of Fig. 3

$$T = T_A + T_B \quad .. \quad .. \quad .. \quad .. \quad (9)$$

The constituent part-periods T_A and T_B have to be calculated separately.

T_A is obtained from the relation [see Figs. 2 and 3 and Equ. (6)]:

$$v_{gB}\Big|_{t_1}^{t_2} = -\,V_{gB}\exp\left(-\frac{t - t_1}{T_{dA}}\right) \quad .. \quad (10)$$

where $v_{gB}\Big|_{t_1}^{t_2}$ signifies the value of v_{gB} during the interval from t_1 to t_2

Let $v_{gc} = v_{gB}$ at $t = t_2$ denote the critical value of grid-control voltage at which commutation in the multivibrator takes place; it is the value of v_{gB} for which $t = t_2$. We then write (see Fig. 3)

$$t_2 - t_1 = T_A \quad .. \quad .. \quad .. \quad (11)$$

We then derive from Equ. (10)

$$T_A = T_{dA}\log_e\frac{V_{gB}}{v_{gc}} \quad .. \quad .. \quad .. \quad (12)$$

Similarly we obtain for T_B with the notation of Fig. 3 and Equ. (8) the expression

$$T_B = T_{dB}\log_e\frac{V_{gA}}{v_{gc}} \quad .. \quad .. \quad .. \quad (13)$$

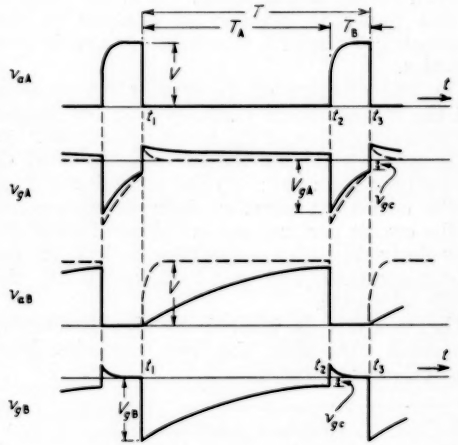

Fig. 3. *Anode and control-grid voltages of the asymmetrical multivibrator. (Notation refers to Fig. 1.)*

v_{aA}, v_{gA} : anode and control-grid voltage of valve V_A.
v_{aB}, v_{gB} : anode and control-grid voltage of valve V_B.
$T_{cB}/T_{dA} \ll 1$ (T_{cB} = time-constant of charging C_B; T_{dA} = time-constant of discharging C_A).

An examination of the simultaneous equations (1) to (4) shows that a general calculation of T_A and T_B is very complex but that a simple solution may be obtained when either $T_{cA}/T_{dB} \ll 1$ or $T_{cB}/T_{dA} \ll 1$. The first condition means that the anode voltage v_{aA} is rectangular or near-rectangular and the second condition that v_{aB} is rectangular or near-rectangular.

Let us assume that $T_{cA}/T_{dB} \ll 1$; i.e., we base our calculations on a rectangular or near-rectangular waveform of v_{aA} as indicated in Fig. 3. The waveform of v_{aB} may be triangular or rectangular as shown in Fig. 3.

The condition $T_{cA}/T_{dB} \ll 1$ means that C_A is virtually charged to the steady supply voltage V at the beginning of the discharge period in the steady state of multivibrator operation. We therefore find from Equ. (1) for V_{gB} (see Equ. VII of the Appendix)

$$V_{gB} = \frac{V}{1 + \frac{r_a}{R_{1A}} + \frac{r_a}{R_{2B}}} \quad .. \quad .. \quad (14)$$

which can be calculated from the given conditions of the circuit and inserted in Equ. (12) to evaluate T_A.

By a line of mathematical reasoning analogous to Equs. (I) to (VII) of the Appendix we obtain from Equ. (4)

$$V_{gA} = \frac{1 - n\left(1 + \frac{r_a}{R_{1B}}\right)}{1 + \frac{r_a}{R_{1B}} + \frac{r_a}{R_{2A}}} V \quad .. \quad .. \quad (15)$$

where n is a temporarily unknown auxiliary quantity of value $0 < n \ll 1$ and defined by the relation

$$V_{cB} = (1 - n)\, V \quad .. \quad .. \quad .. \quad (16)$$

with V_{cB} denoting the voltage across C_B at the beginning of its discharge period.

In order to calculate n we follow the change of voltage across C_B through a complete cycle of events starting with V_{cB} of Equ. (16). C_B first discharges with the time-constant T_{dB}; at the end of the discharge period, T_B, the voltage across C_B is

$$V'_{cB} = V_{cB} \exp\left(-\frac{T_B}{T_{dB}}\right) \quad .. \quad .. \quad (17)$$

In the subsequent charging period, T_A, the voltage rises with the time-constant T_{cB} to

$$V''_{cB} = V - (V - V'_{cB}) \exp\left(-\frac{T_A}{T_{cB}}\right) \quad (18)$$

Since the analysis of the multivibrator performance is made for the steady state of operation we may equate (16) and (18):

$$V''_{cB} = V_{cB} \quad .. \quad .. \quad .. \quad .. \quad (19)$$

and obtain with (17)

$$n = \frac{\exp\left(\frac{T_B}{T_{dB}}\right) - 1}{\exp\left(\frac{T_A}{T_{cB}} + \frac{T_B}{T_{dB}}\right) - 1} \quad .. \quad .. \quad (20)$$

or, by substituting (12) and (13)

$$n = \frac{1 - v_{gc}/V_{gA}}{(V_{gB}/v_{gc})^{T_{dA}/T_{cB}} - v_{gc}/V_{gA}} \quad .. \quad (21)$$

For the further course of calculation it is convenient to have a second expression for n from Equ. (15):

$$n = \frac{1 - \frac{V_{gA}}{V}\left(1 + \frac{r_a}{R_{1B}} + \frac{r_a}{R_{2A}}\right)}{1 + r_a/R_{1B}} \quad .. \quad (22)$$

By equating (21) and (22) the unknown V_{gA} can be found for the evaluation of T_B in Equ. (13).

For practical calculation we usually have $ra \ll R_{1A}$ and $r_a \ll R_{2B}$. This simplifies Equ. (14) to $V_{gB} = V$ and hence (12) to

$$T_A = T_{dA} \log_e \frac{V}{v_{gc}} \quad .. \quad .. \quad .. \quad (23)$$

with, from (6),

$$T_{dA} = C_A R_{2B} \quad .. \quad .. \quad .. \quad .. \quad (24)$$

Further on, $V_{gB} = V$ changes (21) to

$$n = \frac{1 - v_{gc}/V_{gA}}{(V/v_{gc})^{T_{dA}/T_{cB}} - v_{gc}/V_{gA}} \quad .. \quad (25)$$

We may further assume $r_a \ll R_{1B}$ and $r_a \ll R_{2A}$. Equ. (22) then becomes

$$n = 1 - V_{gA}/V \quad .. \quad .. \quad .. \quad (26)$$

which gives with (25)

$$V_{gA} = V - (V - v_{gc})\,(v_{gc}/V)^{T_{dA}/T_{cB}} \quad .. \quad (27)$$

for substitution in (13) to evaluate T_B. From (8) we have for insertion in (13)

$$T_{dB} = C_B R_{2A} \quad .. \quad .. \quad .. \quad .. \quad (28)$$

In practical cases we usually have the condition $V/v_{gc} \gg 1$. This allows (27) to be approximated by a simplified expression and (13) then becomes

$$T_B = T_{dB}\left\{\log_e \frac{V}{v_{gc}} + \log_e\left[1 - \left(\frac{v_{gc}}{V}\right)^{T_{dA}/T_{cB}}\right]\right\} \quad .. \quad .. \quad .. \quad (29)$$

Equ. (9) may thus be written with (23) and (29)

$$T = T_{dB}\left\{\left(1 + \frac{T_{dA}}{T_{dB}}\right)\log_e \frac{V}{v_{gc}} + \log_e\left[1 - \left(\frac{v_{gc}}{V}\right)^{T_{dA}/T_{cB}}\right]\right\} \quad .. \quad (30)$$

In the case of $T_{dA}/T_{cB} \gg 1$ Equ. (29) is simplified to

$$T_B = T_{dB} \log_e (V/v_{gc}) \quad .. \quad .. \quad (31)$$

and (30) to

$$T = T_{dB}(1 + T_{dA}/T_{dB}) \log_e (V/v_{gc}) \quad .. \quad (32)$$

with T_{dA} and T_{dB} given by Equ. (24) and (28) respectively.

Waveforms of Oscillation

The anode voltage v_{aA} shown in Fig. 3 is represented in the time interval t_1 to t_2 by the equation (see Fig. 2),

$$v_{aA}\Big|_{t_1}^{t_2} = r_a\, i_{3A}\Big|_{t_1}^{t_2} \quad .. \quad .. \quad .. \quad (33)$$

and in the time interval t_2 to t_3 by

$$v_{aA}\Big|_{t_2}^{t_3} = V - R_{1A}\, i_{1A}\Big|_{t_2}^{t_3} \quad .. \quad .. \quad (34)$$

Equ. (33) becomes with (III) and (V) of the Appendix

$$\frac{v_{aA}}{V}\Big|_{t_1}^{t_2} = \frac{r_a}{R_{1A}+r_a}\left[1 + \frac{R_{1A}}{R_{2B}\left(1+\frac{r_a}{R_{1A}}+\frac{r_a}{R_{2B}}\right)}\right.$$
$$\left.\exp\left(-\frac{t-t_1}{T_{dA}}\right)\right] \quad .. \quad .. \quad (35)$$

and (34) with (IX) and (XII) of the Appendix

$$\frac{v_{aA}}{V}\Big|_{t_2}^{t_3} = 1 - \frac{C_A R_{1A}}{T_{dA}}\left[1 - \exp\left(-\frac{T_A}{T_{dA}}\right)\right]$$
$$\exp\left(-\frac{t-t_2}{T_{cA}}\right) \quad .. \quad .. \quad (36)$$

The anode voltage v_{aB} shown in Fig. 3 is represented in the time interval t_1 to t_2 by the equation (see Fig. 2),

$$v_{aB}\Big|_{t_1}^{t_2} = V - R_{1B}\, i_{1B}\Big|_{t_1}^{t_2} \quad .. \quad .. \quad (37)$$

and in the time interval t_2 to t_3 by

$$v_{aB}\Big|_{t_2}^{t_3} = r a\, i_{3B}\Big|_{t_2}^{t_3} \quad .. \quad .. \quad .. \quad (38)$$

By mathematical considerations analogous to Equs. (VIII) to (XII) of the Appendix we obtain

$$\frac{v_{aB}}{V}\Big|_{t_1}^{t_2} = 1 - \frac{C_B R_{1B}}{T_{cB}}\left[1 - (1-n)\exp\left(-\frac{T_B}{T_{dB}}\right)\right]$$
$$\exp\left(-\frac{t-t_1}{T_{cB}}\right) \quad .. \quad .. \quad (39)$$

and by analogy to (I) to (V) of the Appendix

$$\frac{v_{aB}}{V}\Big|_{t_2}^{t_3} = \frac{r_a}{R_{1B}+r_a}\left[1 + \frac{R_{1B} - n(R_{1B}+r_a)}{R_{2A}\left(1+\frac{r_a}{R_{1B}}+\frac{r_a}{R_{2A}}\right)}\right.$$
$$\left.\exp\left(-\frac{t-t_2}{T_{dB}}\right)\right] \quad .. \quad .. \quad (40)$$

with n defined by (16) and expressed by (21) or (22).

In practical cases of calculation we usually have $r_a \ll R_{1A}, R_{1B}, R_{2A}, R_{2B}$, and $r_g \ll R_{1A}, R_{1B}, R_{2A}, R_{2B}$. Equs. (35), (36) and (39), (40) may, therefore, be approximated by simplified expressions. Equ. (35) becomes

$$\frac{v_{aA}}{V}\Big|_{t_1}^{t_2} = 0 \quad .. \quad .. \quad .. \quad .. \quad (41)$$

From (40)

$$\frac{v_{aB}}{V}\Big|_{t_2}^{t_3} = 0 \quad .. \quad .. \quad .. \quad .. \quad (42)$$

With the additional practical assumption $V/v_{gc} \gg 1$ Equ. (36) is, with (23), approximated by

$$\frac{v_{aA}}{V}\Big|_{t_2}^{t_3} = 1 - \exp\left(-\frac{t-t_2}{T_{cA}}\right) \quad .. \quad (43)$$

with, from (5),

$$T_{cA} = C_A R_{1A} \quad .. \quad .. \quad .. \quad .. \quad (44)$$

Equ. (39), with (13) and (26), is approximated by

$$\frac{v_{aB}}{V}\Big|_{t_1}^{t_2} = 1 - \exp\left(-\frac{t-t_1}{T_{cB}}\right) \quad .. \quad (45)$$

with, from (7),

$$T_{cB} = C_B R_{1B} \quad .. \quad .. \quad .. \quad .. \quad (46)$$

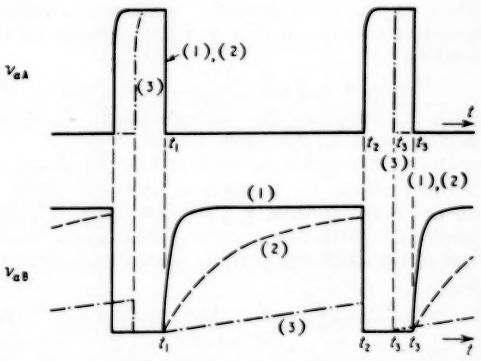

Fig. 4. *Theoretical waveforms of asymmetrical multivibrator oscillation computed from Equs.* (41) *to* (46).
(1) $T_{cB}/T_{dA} = 0.1$; (2) $T_{cB}/T_{dA} = 1$; (3) $T_{cB}/T_{dA} = 10$.

Experiments

Experiments were made to test Equ. (30) for the frequency of multivibrator oscillation and Equs. (41) to (46) for the waveform. The pentodes used were VR56 = EF6 with $r_a = 2200\ \Omega$, $r_g = 1100\ \Omega$, and $v_{gc} = 5.2$ V (100 V at the screen-grid). The steady supply voltage V was 100 V.

The following circuit values were used :

$R_{1A} = 50\ \text{k}\Omega$, $R_{2A} = 50\ \text{k}\Omega$, $R_{2B} = 2\ \text{M}\Omega$.

(1) $R_{1B} = 20\ \text{k}\Omega$; (2) $R_{1B} = 200\ \text{k}\Omega$; (3) $R_{1B} = 2\ \text{M}\Omega$.

(a) $C_A = 0.005\ \mu\text{F}$; $C_B = 0.05\ \mu\text{F}$.

(b) $C_A = 0.001\ \mu\text{F}$; $C_B = 0.01\ \mu\text{F}$.

The frequencies computed from Equ. (30 are :

(1a) : 27.2 c/s	(1b) : 136 c/s
(2a) : 27.2 c/s	(2b) : 136 c/s
(3a) : 29.8 c/s	(3b) : 149 c/s

The experimental frequencies measured with an accuracy of about 2% were :

(1a) : 27 c/s	(1b) : 135 c/s
(2a) : 27 c/s	(2b) : 135 c/s
(3a) : 29.4 c/s	(3b) : 147 c/s

The discrepancy between experiment and theory is small.

Fig. 4 shows the theoretical waveforms computed from Equs. (41) to (46). The waveforms are the same for both cases (a) and (b). The oscillograms in Fig. 5 verify the theoretical predictions.

Conclusion

Fig. 4 illustrates the conclusions to be derived from Equs. (30) and (41) to (46) with respect to the frequency and waveform of the asymmetrical multivibrator.

The frequency of oscillation may be altered, without affecting the waveform, by changing the capacitances but keeping constant the capacitance ratio. The wave-form of the 'unrestricted' anode voltage may be varied from rectangular to 'curved'-triangular without affecting the frequency of oscillation or the spacing of the oscillation sections; the change of waveform is obtained by increasing the associated anode resistance but keeping fixed the other circuit values, [see curves (1) and (2) of Fig. 4]. If the anode resistance is considerably increased then the anode voltage tends to become 'linear'-triangular and the frequency of oscillation tends to rise [see curve (3) of Fig. 4].

Design

Valve data and supply voltage V are as before. Wanted : $f = 250$ c/s with rectangular waveforms and $T_A/T_B = 3$ (for notation see Fig. 3).

From the data given we have $T = 0.004$ sec, $T_A = 0.003$ sec and $T_B = 0.001$ sec. Further, $V = 100$ V and $v_{gc} = 5.2$ V.

Rectangular waveforms mean that $T_{cB}/T_{dA} \ll 1$ and $T_{cA}/T_{dB} \ll 1$ and that consequently Equs. (23) and (31) are applicable. With (24) and (28) we obtain, respectively,

$$C_A R_{2B} = \frac{T_A}{\log_e \frac{V}{v_{gc}}} = 0.001 \text{ sec} \quad .. \quad (a)$$

and

$$C_B R_{2A} = \frac{T_B}{\log_e \frac{V}{v_{gc}}} = 0.00034 \text{ sec} \quad .. \quad (b)$$

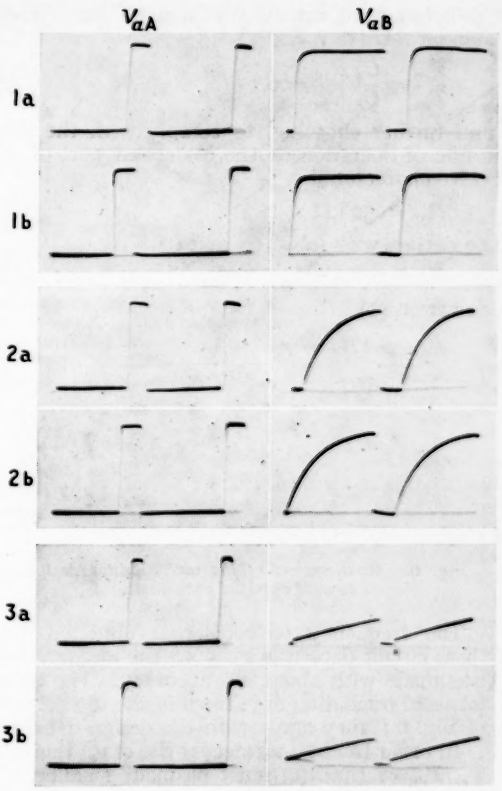

Fig. 5. *Oscillograms of v_{aA} and v_{aB} corresponding to the theoretical waveforms of Fig. 4.*
(1) $T_{cB}/T_{dA} = 0.1$; (2) $T_{cB}/T_{dA} = 1$; (3) $T_{cB}/T_{dA} = 10$; (a) $C_A = 0.005$ μF *and* $C_B = 0.05$μF ; (b) $C_A = 0.001$ μF *and* $C_B = 0.01$ μF. *The measured frequencies are* (1a), 27 *c/s* ; (1b), 135 *c/s* ; (2a), 27 *c/s* ; (2b), 135 *c/s* ; (3a), 29.4 *c/s* ; (3b), 147 *c/s*.

Choosing, in view of the rectangular waveform of v_{aA},

$$\frac{T_{cA}}{T_{dB}} = \frac{C_A R_{1A}}{C_B R_{2A}} = 0.1 \quad .. \quad .. \quad .. \quad (c)$$

and further choosing, to comply with the condition of operation on the coalescent part of the valve characteristic,

$$R_{1A} = 34 \text{ k}\Omega \quad .. \quad .. \quad .. \quad .. \quad (d)$$

we obtain

$$R_{2B} = 1 \text{ M}\Omega \quad .. \quad .. \quad .. \quad .. \quad (e)$$

and

$$C_A = 0.001 \text{ } \mu\text{F}. \quad .. \quad .. \quad .. \quad (f)$$

Choosing, to satisfy the demand for a rectangular form of v_{aB},

$$\frac{T_{cB}}{T_{dA}} = \frac{C_B R_{1B}}{C_A R_{2B}} = 0.1 \quad .. \quad .. \quad .. \quad (g)$$

and further choosing, to comply with the condition of operation on the coalescent part of the valve characteristic,

$$R_{1B} = 50\ \text{k}\Omega \quad .. \quad .. \quad .. \quad .. \quad (h)$$

we derive, with (a) or (e) and (f),

$$C_B = 0.002\ \mu\text{F} \quad .. \quad .. \quad .. \quad .. \quad (i)$$

and from (b)

$$R_{2A} = 170\ \text{k}\Omega \quad .. \quad .. \quad .. \quad .. \quad (j)$$

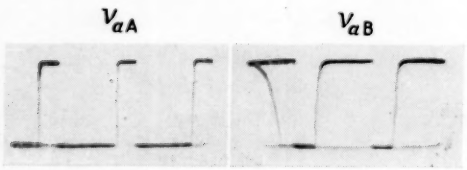

Fig. 6. *Oscillograms of the multivibrator designed to meet specified conditions.*

The frequency of oscillation obtained with these circuit data was 252 c/s; the measurement was made with about 2% accuracy. The waveforms of oscillation are shown in the oscillograms of Fig. 6; they agree with the design demands.

In order to obtain a steeper rise of v_{aA} the ratio T_{cA}/T_{dB} of Equ. (c) must be made smaller, and for a steeper rise of v_{aB} the ratio T_{cB}/T_{dA} of Equ. (g) must be reduced.

REFERENCE

[1] R. Feinberg, "Symmetrical Multivibrators", *Wireless Engineer*, May 1949, Vol. 16, p. 153.

APPENDIX

From Equ. (1) with (6) we obtain

$$\frac{di_{2A}}{dt} = -\frac{1}{T_{dA}} i_{2A} \quad .. \quad .. \quad .. \quad .. \quad (I)$$

and, therefore, for the time interval t_1 to t_2, see Fig. 3:

$$i_{2A}\Big|_{t_1}^{t_2} = K_1 \exp\left(-\frac{t - t_1}{T_{dA}}\right) \quad .. \quad .. \quad (II)$$

and

$$i_{3A}\Big|_{t_1}^{t_2} = \frac{V}{R_{1A} + r_a} + \frac{R_{1A}}{R_{1A} + r_a} K_1 \exp\left(-\frac{t - t_1}{T_{dA}}\right) \quad .. \quad .. \quad .. \quad (III)$$

With the notation of Fig. 2 the voltage v_{cA} across C_A is, in the time t_1 to t_2,

$$v_{cA}\Big|_{t_1}^{t_2} = r_a\, i_{3A}\Big|_{t_1}^{t_2} + R_{2B}\, i_{2A}\Big|_{t_1}^{t_2} \quad .. \quad .. \quad (IV)$$

The condition $T_{cA}/T_{dB} \ll 1$ means that $v_{cA} = V$ when $t = t_1$; we thus obtain for the integration constant K_1

$$K_1 = \frac{V}{R_{2B}\left(1 + \frac{r_a}{R_{1A}} + \frac{r_a}{R_{2B}}\right)} \quad .. \quad .. \quad (V)$$

Since, from Fig. 2 and Equ. (10)

$$V_{gB} = -v_{gB} = R_{2B}\, i_{2A} \text{ when } t = t_1 \quad .. \quad (VI)$$

we obtain with (II) and (V)

$$V_{gB} = \frac{V}{1 + \frac{r_a}{R_{1A}} + \frac{r_a}{R_{2B}}} \quad .. \quad .. \quad (VII)$$

From Equ. (3) we obtain with (5)

$$\frac{di_{1A}}{dt} = -\frac{1}{T_{cA}} i_{1A} \quad .. \quad .. \quad .. \quad .. \quad (VIII)$$

and, therefore, for the time interval t_2 to t_3, see Fig. 3:

$$i_{1A}\Big|_{t_2}^{t_3} = K_2 \exp\left(-\frac{t - t_2}{T_{cA}}\right) \quad .. \quad .. \quad (IX)$$

With the notation of Fig. 2 the voltage v_{cA} across C_A is in the time t_2 to t_3 (switch S being in position B):

$$v_{cA}\Big|_{t_2}^{t_3} = V - \left(R_{1A} + \frac{R_{2B}\, r_g}{R_{2B} + r_g}\right) i_{1A}\Big|_{t_2}^{t_3} \quad .. \quad (X)$$

The condition $T_{cA}/T_{dB} \ll 1$ means that virtually $v_{cA} = V$ at $t = t_1$ and hence

$$v_{cA} = V \exp\left(-\frac{T_A}{T_{dA}}\right) \text{ for } t = t_2 \quad .. \quad .. \quad (XI)$$

Equs. (IX) to (XI), therefore, give for the integration constant with Equ. (5)

$$K_2 = V \frac{C_A}{T_{cA}}\left[1 - \exp\left(-\frac{T_A}{T_{dA}}\right)\right] \quad .. \quad .. \quad (XII)$$

ELECTRONICS SYMPOSIUM

The Electronics Section of the Scientific Instrument Manufacturers' Association will hold a symposium from 2nd to 4th November 1949 at the Examination Hall, Queens Square, London, W.C.1 In addition to a display of scientific instruments there will be papers on "Electronic Instrumentation in Atomic Research," by Dr. Dennis Taylor; "Electronic Amplifiers," by P. S. Blackman; "Magnetic Amplifiers," by A. V. Hemingway; "Some Recent Improvements in Electronic Measuring Technique," by C. H. W. Brookes-Smith and J. A. Collis; "The Measurement of Some Transient Phenomena," by Dr. H. A. Dell; "An Industrial Electronic Servo-Mechanism," by P. H. Briggs and "Co-operative Research at B.S.I.R.A.", by Dr. A. J. Maddock.

Entrance to the symposium is by ticket, obtainable from the Secretary of the Scientific Instrument Manufacturers' Association.

OBITUARY

It is with regret that we record the death of Captain A. G. D. West, M.A., B.Sc., in a climbing accident in Switzerland on 22nd August. He was managing director of Cinema Television and vice-president of the International Television Committee.

In 1923 he joined the B.B.C. at the age of 26, leaving it in 1929 to become chief of design and development for the Gramophone Co. In 1933 he became technical director of Baird Television (now Cinema Television). He was president of the British Kinematograph Society from 1938 to 1946.

CHANGE OF MUTUAL CONDUCTANCE WITH FREQUENCY

Effect of Oxide-Coated Cathode

By Walter Raudorf

SUMMARY.—The mutual conductance of indirectly-heated cathode receiving valves varies with frequency after about a thousand operating hours. This phenomenon is due to the deterioration during operation of the contact between the oxide coating and the metal sleeve which forms the core of the cathode. It can be greatly reduced by giving the metal sleeve an appropriate shape. By applying Holm's theory of electric contacts it is possible to estimate the number and size of the contact spots (a-spots) between coating and core metal. For an average size of 3μ for the oxide grain, for instance, and a contact resistance of about 40Ω per cm^2 of the cathode surface, the number of a-spots is about 3×10^4 per cm^2 and their average diameter about 1μ. The contact resistance and the liability to cathode sparking seem to be connected. In general, cathode sparking is unlikely up to a specific emission of 1 A/cm^2. To prevent sparking at pulse currents of 10 A/cm^2 of less than 1 msec duration, the contact resistance between coating and core must be less than $10\Omega/cm^2$.

Introduction

IT has been found that, in the course of operation, amplifiers equipped with valves having indirectly-heated cathodes show a variation of the original frequency response. Measurements of the mutual conductance g_m as dependent on operating time at low ($<10^5$ c/s) and high ($>10^7$ c/s) frequencies proved that this variation is caused by the valves. It appears that values of g_m obtained at low frequencies drop more quickly with operating time than those at high frequencies. Consequently the frequency response of the mutual conductance of the valves, and thus of the gain of the amplifier, changes at an increasing rate with advancing operating time.

Nature and Cause of the Change of g_m

In an attempt to explain the effect, the variation of gain with frequency was measured for a number of valves and the measurements were repeated at considerable intervals of time. The results differ qualitatively only to an insignificant degree. New valves in general exhibit no frequency response or very little; after about 1,000 hours of operation the frequency dependence of g_m becomes obvious and increases in the course of further operation. After about 3,000 hours the frequency response remains almost unchanged. The frequency curves of the gain of a test valve V_{12} at different stages in its life are given in Fig. 1 and serve to illustrate this behaviour. The resistive load R_L in these experiments was small compared with the anode resistance r_a of the valve, so that the gain s in nepers is given sufficiently accurately by

$$s = \log_e |g_m R_L|,$$

MS accepted by the Editor, January 1949

where g_m has a complex value. The flat response below 10^5 c/s and above 10^7 c/s, is typical and indicates s = constant for $\omega \to 0$ and $\omega \to \infty$, ω being the angular frequency. From these curves one gathers that during operation an impedance is somehow formed in the cathode circuit, which consists of a resistance shunted by a capacitance, and that this impedance causes a frequency-dependent mutual conductance and gain. The following procedure was adopted to confirm this assumption.

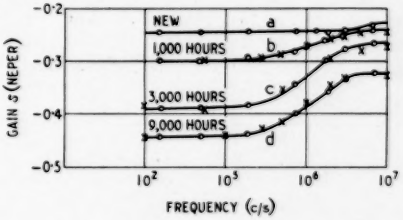

Fig. 1. *Variation of gain with frequency at different periods in the life of a test valve* V_{12}.
—o—o— *measured.* × × × *calculated.*
The values for R and C of the equivalent circuit of Fig. 2 used in the calculations were: curve (b) $R = 6\ \Omega$, $C = 1.9 \times 10^4$pF; *curve (c)* $R = 14\Omega$, $C = 1.3 \times 10^4$pF; *curve (d)* $R = 17\Omega$, $C = 1.2 \times 10^4$pF.

If R in the equivalent circuit (Fig. 2) represents the resistance between the oxide coating and the core metal, C the shunting capacitance, g_m^0 the mutual conductance for $R = 0$, then the mutual conductance for $R > 0$ and $R_L \ll r_a$ is given by

$$g_m = \frac{g_m^0}{1 + \dfrac{R\, g_m^0}{1 + j\omega CR}}$$

and its absolute value

$$|g_m| = g_m{}^0 \sqrt{\frac{1 + \omega^2 R^2 C^2}{(1 + R\, g_m{}^0)^2 + \omega^2 R^2 C^2}} \quad .. \quad (1)$$

and for the gain in nepers

$$s = \log_e |g_m R_L| = \log_e \sqrt{\frac{1 + \omega^2 R^2 C^2}{(1 + R g_m{}^0)^2 + \omega^2 R^2 C^2}} + \log_e (g_m{}^0 R_L) \quad .. \quad .. \quad .. \quad (2)$$

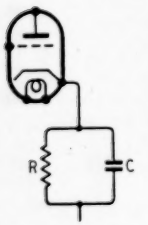

Fig. 2. *Equivalent circuit.*

By measuring the gain at three different frequencies and substituting the found values in (2) one obtains three equations from which the unknowns $g_m{}^0$, R and C can be determined for a particular valve. Taking $\omega_1 = 0$, $\omega_2 = 5 \times 10^6$, $\omega_3 = 10^8$ c/s, these magnitudes were computed for the test valve V_{12}, and by substituting the values obtained in (2), the frequency response of the gain was calculated. The experimentally found gain curves are recorded in Fig. 1; the crosses along the curves mark the calculated values and obviously agree well with the measured values. The values of C and R used in the calculations for each curve are shown in Fig. 1.

In all the other cases which were investigated a satisfactory agreement between measurement and calculation was observed. The values of C and R ascertained in this way, some of which are given in the Table 1 will be discussed later.

TABLE I

Valve	Surface of the coating (cm²)	Hours of operation	R (Ω)	C (pF)
				$\times 10^4$
V_{12}	1.9	1000	6	1.9
V_{12}	,,	3000	14	1.3
V_{12}	,,	9000	17	1.2
V_{10}	,,	5000	20	2.1
V_{11}	,,	5000	19	2.8
V_{14}	,,	5000	28	2.3
V_{15}	,,	5000	23	2.0
V_{17}	,,	5000	32	2.8
V_{18}	,,	3000	24	0.9
V_{20}	,,	3000	21	0.5

Calculated values of resistance and capacitance which constitute the cathode impedance at different periods of operation.

Incidentally it may be mentioned that the value of R can also be approximately determined by another simple method. Operating the valve as a diode, one measures the anode conductance g_a at currents I_a as high as possible and plots $1/g_a$ versus $1/I_a$ (Fig. 3). In the ideal case $1/g_a$ and $1/I_a$ approach zero together; actually, however, $1/g_a$ approaches R. As $1/I_a = 0$ cannot in practice be realized, the value of R must be extrapolated. This, of course, involves inaccuracies, apart from the effects due to inactivity of the cathode, which become particularly apparent at high specific emissions. Nevertheless this direct method provides approximations which are not contradictory to the results obtained by the indirect method.

Thus it seems justifiable to explain the variation of the frequency response of the gain by a frequency dependent negative feedback, caused by an impedance in the cathode circuit which arises in the course of operation.

The question now is where and how does such an impedance develop. One tends to assume that as the activity of the cathode drops with increasing operating time, the conductivity falls off as well, and consequently a resistance occurs in the coating which is shunted by the capacitance between the surface of the oxide coating and the metal sleeve. The assumption, however, proved to be wrong. Neither an obvious influence of the thickness of the coating on the frequency response nor a definite relationship between the activity and the frequency curve could be found. It is true that valves showing a considerable dependence of g_m on frequency usually show a more or less lack of cathode activity as well; inactive valves, however, do not always show a frequency dependent mutual conductance. Measurements carried out on special valves ultimately proved that the resistance across the oxide coating changes only little in the course of the life of the valve, and remains below 2 ohms per cm² even after several thousand hours of operation. Actually, however, R of the test valves was found on an average to be about 40 ohms per cm² of the coating surface. As to capacitance between coating and metal sleeve, measurements on the cold cathode resulted in at the most 150 pF/cm² for a thickness of coating of about 30μ. The value of C, however, obtained from the frequency curves amounts to the order of 10^4 pF/cm² (see Table I), which means that the distance between the surfaces constituting the capacitor across R must be smaller than 1μ.

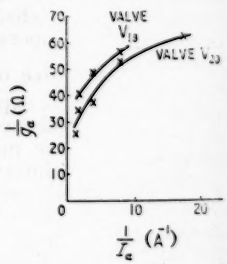

Fig. 3. $\frac{1}{g_a}$ *versus* $\frac{1}{I_a}$ *after* 3,000 *operating hours.*

The unexpectedly high values of C and R indicate that the dependency on frequency of the mutual conductance and gain, must be a process localized to the interface between oxide layer and core, which gives rise to the impedance above mentioned. Investigations in this direction finally led to the result that such a process actually occurs during operation, and that this process is of a mechanical nature. This can be described in detail with the aid of Fig. 4.

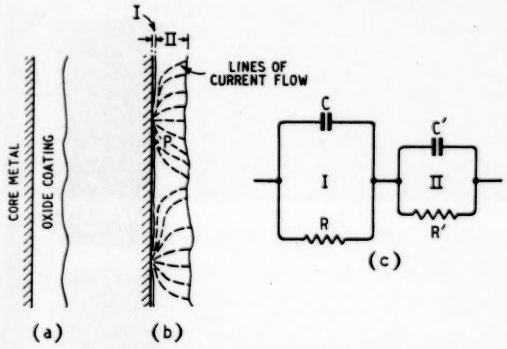

Fig. 4. *Diagrammatical representation of the development of the contact resistance between oxide coating and core; (a) new valve, (b) after aging, (c) equivalent circuit.*

In a new valve the contact between emissive coating and core metal is good [Fig. 4(a)] and the contact resistance negligibly small. During the lifetime of the valve the real contact surface becomes smaller for reasons which are still to be investigated, and thus the electrical contact deteriorates [Fig. 4(b)], so that the contact resistance increases considerably and becomes great compared with the resistance across the oxide layer. The lines of current flow, at the ends of which the potentials occur during operation, are forced to run as indicated in Fig. 4(b) (current constriction). Consequently a comparatively high tension arises on some parts of the inner boundary surface of the coating, for instance at P, when the valve is operated. The total area of all these parts, together with the adjacent parts of the core metal, forms a capacitor with a minute plate distance ($< 1\,\mu$) parallel to the contact resistance R. In this way the impedance Z, which is responsible for the variation of the frequency response of the gain, originates in the interface between coating and core [Fig. 4(b), zone I]. In series with this impedance Z lies another impedance Z' in association with zone II [Fig. 4(b)] which is due to the resistance of the coating R' and the capacitance C' between outer and inner surface of coating. The equivalent circuit of the cathode, therefore, is as illustrated in Fig. 4(c). In the case of old valves it is usual to find $R' \ll R$ and $C' \ll C$, therefore, the impedance Z' can be neglected in the calculation of the frequency response.

During the course of the investigations on the cathode impedance Z, the shape of the core proved to have a decisive effect on the formation of the contact resistance R, in comparison with which all other influences were of minor importance. It appears that the undesired frequency response becomes the more pronounced, the greater the curvature of the core surface. Fig. 5, shows the variation of the gain with operating time as measured on valves with flat cathodes in comparison with those with round cathodes. The term

$$\Delta s = (s_{20} - s_{0\cdot25})_t - (s_{20} - s_{0\cdot25})_0$$

serves as a measure of the change of frequency response with time; i.e., the difference of the gain at 20 and 0.25 Mc/s after t hours of operating minus the difference of the gain at the start of the operation. In Fig. 5, t denotes the hours of 'rapid aging.' 'Rapid aging' was introduced to accelerate investigations, and is a special way of operating with a considerably-overheated cathode which produces or alters, the frequency response within a considerably shorter time than aging under normal conditions. The choice of the frequencies $f_1 = 0.25$ Mc/s and $f_2 = 20$ Mc/s, which might appear to be arbitrary, is justified by the course of the frequency curves in Fig. 1.

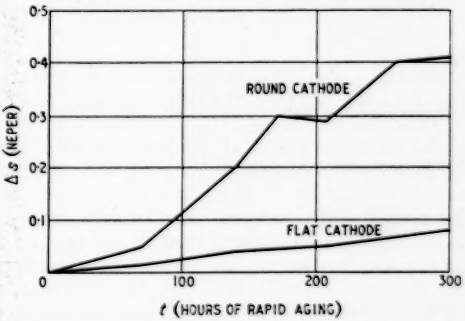

Fig. 5. *Variation of the gain with operating time, measured on valves with round and with flat cathodes (average values).*

To choose f_1 somewhere below 100 kc/s would, in fact, be more suitable, for if $f_1 < 100$ kc/s, $f_2 > 20$ Mc/s Δs would be determined by the given formula nearly independent of frequency. Unfortunately, however, the available test set did not supply frequencies much below 250 kc/s.

The improved behaviour of flat cathodes was

confirmed by measurements on a range of suitable valve specimens.

The results of the electrical measurements obtained on round and flat cathodes are in full agreement with optical tests. Figs. 6 and 7 show the typical appearance of emission surfaces of both kinds of cathodes immediately after their formation, and after 2000 hours of operation. The influence of the surface curvature of the core is obvious. Although the original composition of the emissive material, the method of coating, the process of exhausting, forming and activating were the same in all cases, the oxide coatings on the round cores exhibit considerably more and larger cracks after aging than those on the flat cores. The reason probably is that, when applying the carbonate to the core by spraying, the particles hit the surface of the metal sleeve predominantly at right angles in the case of the flat core, and consequently adhere better than in the case of the round core where the angles of incidence can have all possible values between 0 and 90°.

It will be understood that the contact between the coating and core deteriorates as the cracks in the coating increase during the life of the valve. That the frequency response remains more or less unchanged after a certain operating time is comprehensible, since the structure of the coating will not alter when enough cracks have developed to relax the strains and stresses in the coating.

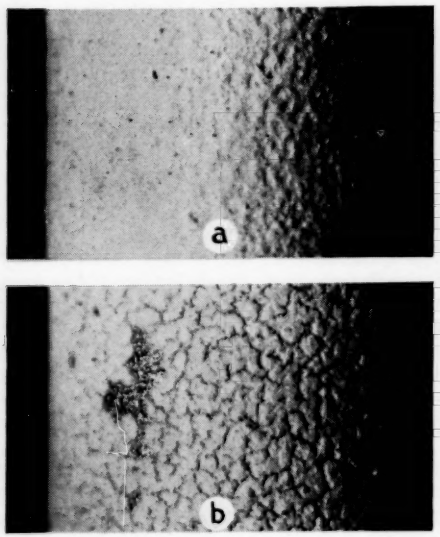

Fig. 6. *Emission surface of a round cathode* (25x); *(a) immediately after formation, (b) after 2,000 hours of operation.*

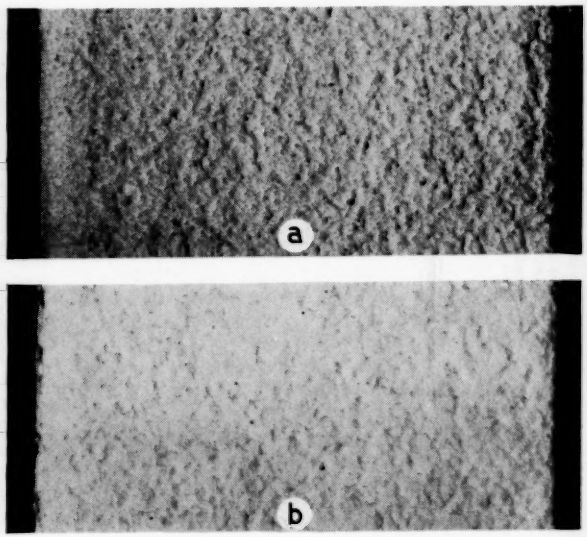

Fig. 7. *Emission surface of a flat cathode* (25x); *(a) immediately after formation, (b) after 2,000 hours of operation.*

Size of a-Spots

In order to explain the frequency response of the mutual conductance and its variation with time, it has been assumed that the boundary surfaces between coating and core do not touch everywhere but only on minute contact areas. The actual contact surface, therefore, is composed of all the minute contact areas, whereas the considerably larger area of the interface represents only the apparent contact surface. The narrow areas through which the lines of current flow are bent together cause an increase of resistance, called constriction resistance or contact resistance, (Holm[1]), compared with the case of a fully conducting apparent contact surface. Applying Holm's formulae for contact resistances it is possible to estimate the number of contact surfaces (a-spots) as dependent upon the contact resistance, on the following assumptions:

1. The resistance of the core metal (Ni) is negligible in comparison with that of the coating.
2. The main part of the contact resistance is localized in the immediate neighbourhood of the microscopic conducting spots (a-spots).
3. The distribution of the a-spots is regarded as uniform.

4. The contact surfaces are clean (i.e., there are no alien films on the contact members) so that the current passes without any transition resistance in the interface.

5. The restivity of the coating is independent of the position.

6. The thickness of the coating is very small compared with the thickness of the core, so that the problem can be considered as two dimensional.

As previously pointed out, the resistance R' across the coating [Fig. 4(c)] of a thickness δ and a resistivity ρ turns out to be very small compared with the contact resistance R located at the interface. For this reason and because R' appears in the measurement in the same way as R, the expression 'contact resistance' is used in the following for the total resistance between the coating and the core metal.

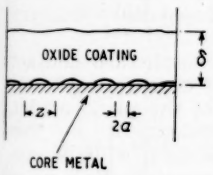

Fig. 8. *Diagram of section through apparent contact surface.*

If R now denotes the contact resistance per unit area of the cathode surface, n the number of a-spots (Fig. 8) per unit area of the apparent contact surface, and πa^2 the average area of the a-spots, ($2a$ being the mean diameter) the contact resistance per cm² is given by

$$R = \rho\delta + \frac{0.9}{n}\frac{\rho}{2\pi a}\tan^{-1}\frac{0.9}{a\sqrt{n\pi}} - \rho\frac{0.9}{\sqrt{n\pi}} \quad (4)$$

Assuming a, δ and ρ to be given, then (4) provides the required relationship between R and n. Substituting in (4), $\delta = 30\mu$ and for the resistivity ρ of formated BaO at 700°C, according to Mayer and Schmidt[2] 240Ω cm, one obtains a relationship between R, n, z and a as set out graphically in Fig. 9. The number n of the a-spots and the distance $z = 1/\sqrt{n}$ from centre to centre of the a-spots are plotted versus R with the mean radius a of the a-spots as parameter.

The question now is to find a plausible value for a. Assuming a structure of the coating according to Benjamin, Huck and Jenkins[3] (as illustrated in Fig. 10) the mean diameter $2a$ of the a-spots appears to be smaller than the largest dimension of an average particle. In the test valves, the particles were of the order of 3μ in size, and the thickness of the coating was about 10 times that value. Consequently a was smaller than δ by at least one order of magnitude.

For such a small value of a the following fact must also be considered. The larger the a-spots are assumed to be for a given contact resistance R, the greater their distance from centre to centre becomes, since n decreases with increasing a, and $z = 1/\sqrt{n}$. If z becomes a multiple of the thickness of the coating, a flaking off of the oxide is probable. Actually a flaking off was not observed on the test cathodes under normal operating conditions up to $R = 40\Omega/\text{cm}^2$. The value of a, therefore, must be assumed to be such as to make a flaking-off of the coating unlikely as long as $R < 40\Omega/\text{cm}^2$, that means $z \leqslant p\delta$, where p is a factor, the value of which must be ascertained empirically. In the case of the test cathodes, for instance, p turned out to be approximately 3.

There is also a lower limit to a. The best possible contact between coating and core occurs if the metal surface of the core is covered coherently with oxide particles, each particle touching the core. In this case the average distance z from centre to centre of the a-spots equals the size of the grain; z can never fall below this value even if R approaches the resistance $\rho\,\delta$ of the coating. Therefore, the relation $z \geqslant g$ always holds, where g denotes the average size of the grain. Putting $g = 3\mu$, $\delta = 30\mu$, $p = 3$, in accordance with the actual test conditions, the following inequality results:

$$3\mu \leqslant z \leqslant 90\mu \quad .. \quad .. \quad .. \quad .. \quad (5)$$

which is valid within the range of the values of

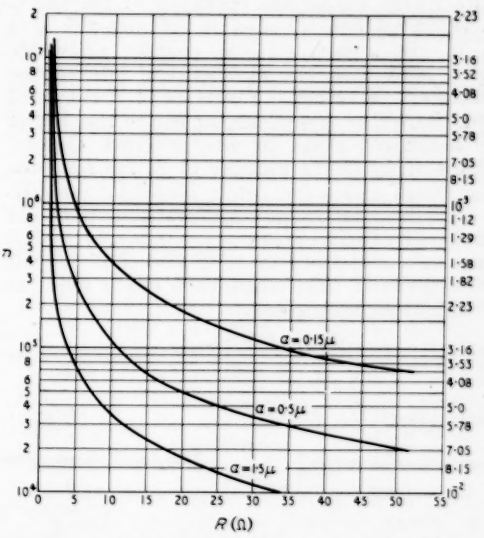

Fig. 9. *The number n of a-spots per cm² and the distance $z = 1/\sqrt{n}$ from centre to centre of the a-spots versus contact resistance R per cm²; the average radius a of the a-spots being the parameter.*

R considered; i.e., from the lowest observed value $R =$ about $1\Omega/cm^2$ to $R = 40\Omega/cm^2$. The z/R curves in Fig. 9, show that z exceeds the upper limit at $R = 40\Omega/cm^2$, if the diameter of the a-surfaces is assumed to equal the size of the grain. If it is supposed to be of lesser order than the grain, (e.g., $2a = 0.30\mu$) then the left side of (5) is no longer satisfied. Consequently the diameter of the a-surfaces lies on the average between 0.3 and 3μ. As a matter of fact all values of z within the considered interval of R satisfy (5) if $2a$ is assumed to be 1μ.

Fig. 10. *Diagram of section through coating-core metal.*

The contact resistance of virgin cathodes with circular cross section was $5\Omega/cm^2$ on the average, and went up to $40\Omega/cm^2$ in the course of several thousand operating hours. This increase of R has been explained by the decrease of the actual contact area during the operation of the valve. As the total contact area is actually the area of all the a-surfaces, the contact resistance varies both with the number and size of the a-surfaces. Whether the increase of R is caused by a change in area alone, or in the number of the a-surfaces alone, or whether both changes share equally in the increase of R, has not been ascertained. However, it is obvious from Fig. 9 and the preceding considerations that the number of a-surfaces per cm^2 lies in most practical cases in the vicinity of 10^5; i.e., it is roughly two orders less than where each of the adjacent particles touches the core.

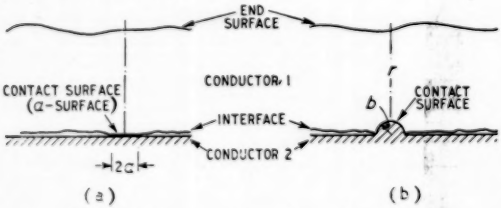

Fig. 11. *(a) Plane contact model; (b) contact model, of spherical symmetry.*

Sparking

When an oxide-coated cathode valve passes more than a certain amount of current, a phenomenon called 'sparking' occurs. This phenomenon limits the overload capacity of such cathodes, and appears in the form of an incandescent spot on the coated cathode, resulting in a vaporization or explosion of a part of the coating. Such action causes an irreparable destruction of the cathode or a portion of it (Knowles and McNall[4]). It seems probable that cathode sparking is a heating phenomenon, and one can attempt to explain it by electrical heating of the construction region in the oxide coating. The development of temperature in the warmest section of a current constriction is of special interest, if at a given instant a certain constant current is drawn from the cathode.

Because of mathematical difficulties the theoretical treatment of this problem is not successful in the case of plane contact surfaces [Fig. 11(a)]. It is possible, however, to solve the problem in the case of contact surfaces of spherical symmetry as shown in Fig. 11(b).

If the radius b of the hemispherical contact surface is such that the same constriction resistance occurs as in the case of the plane model, then the temperature development in this resistance will be approximately the same in both cases (Fink and Körner).[5]

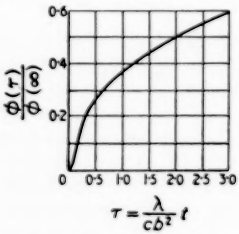

Fig. 12. *Initial temperature development in the warmest section of a contact constricted according to Fig. 11(b), after current start.*

The development of temperature in a spherically-symmetrical current constriction has been treated by Holm[1] under the following simplifying conditions:

1. Conductor 1 [Fig. 11(b)] is a fairly good conductor, 2 a perfect electrical conductor.

2. The 'end surfaces' lie at large distances from the contact surface; i.e., $r \gg b$.

3. The electrical resistivity ρ, the thermal conductivity λ, and the heat capacity c, referred to unit volume, are constant.

4. At the instant $t = 0$ (i.e., at current start), the super-temperature θ (i.e., the increase of temperature of the contact surface), is everywhere zero, the zero point being the temperature of the main body of the contact member.

5. When $t > 0$ the super-temperature θ remains equal to 0 at $r = b$ and at the end surfaces $r \gg b$.

With regard to the boundary conditions 4 and 5, the warmest section is determined by $r = 2b$ (Holm).[1] If $\phi(\tau)$ denotes the super-temperature as a function of the reduced unit of time $\tau = \frac{\lambda}{cb^2} t$ and $\phi(\infty)$ the super-temperature of the warmest section in the permanent state, then $\frac{\phi(\tau)}{\phi(\infty)}$ as function of τ gives the course of the

temperature in the warmest section for any conductor 1 (Fig. 12).

By means of the relation $b = a/\sqrt{2.47}$, which results from the equalization of the constriction resistances in the plane model and the spherically symmetrical model, the solution illustrated by the graph in Fig. 12 can be evaluated for the plane model, provided that a, ρ, λ, and c are known.

In this way the groups in Figs. 13–17 were obtained, the contact resistance R and the emission current I_{em} per cm² of the cathode surface being the parameters. As a mean diameter of the a-surfaces 1μ was chosen; the values of ρ, λ, and c were taken from the literature; $\rho = 240\Omega$ cm (Ref. 2), $\lambda = 0.0025$ watt/cm/degree (Ref. 6), $c = 2.4$ watt/cm³/degree (Ref. 7).

Owing to the simplifying assumptions on which the calculations are based, the solutions set out by the graphs apply only to short periods of emission, and even then only approximately. For currents lasting longer than a few milliseconds the actual temperature might lie considerably below those calculated, particularly so because of the neglected 'cooling effect'[8] and the heat radiation of the oxide.

With regard to the data on the speed of evaporation of BaO determined by Claassen-Veenemans,[9] the temperature in the warmest section of the coating at which cathode sparking occurs probably lies in the vicinity of the melting point of BaO; i.e., according to Schuhmacher[10] 2196° K. Such a temperature, for instance, is reached within 1 msec according to the θ/t curves in Fig. 17, assuming a contact resistance of $R = 10\Omega/\text{cm}^2$, an emission of 10 A/cm², and an operating temperature of the cathode of 1000° K. Up to currents of $I_{em} = 1\text{A/cm}^2$, however, sparking is unlikely, since contact resistances above $60\Omega/\text{cm}^2$ are in practice out of question. If sparking should nevertheless occur, it would probably be due to irregularities in the oxide layer. Usually the emission is not as uniformly distributed over the cathode as was assumed for the calculation. The most active spots carry, of course, most of the current, and consequently get overloaded to such an extent that cathode sparking occurs already at comparatively low currents. In the case of very-short current pulses, it is conceivable that a capacitance of the order of 10^4 pF/cm², which shunts the contact resistance, prevents current constriction, and consequently sparking might not occur in spite of highest emission.

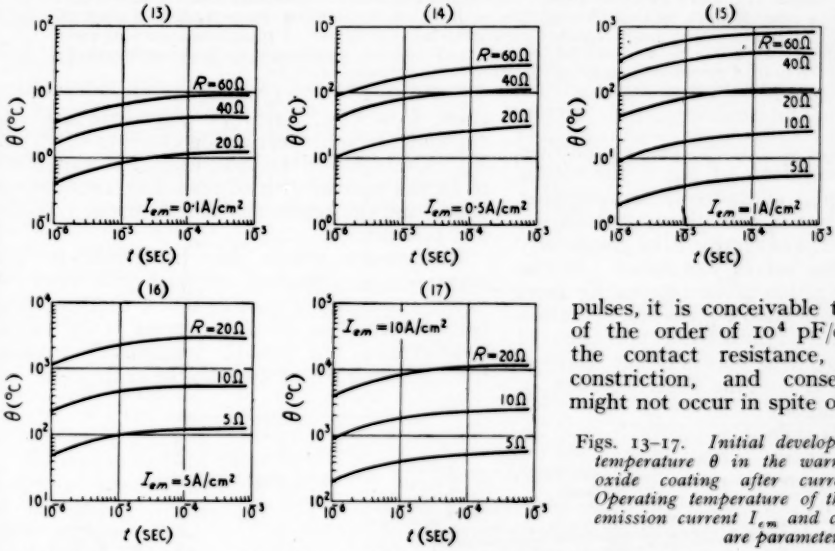

Figs. 13–17. *Initial development of the super-temperature θ in the warmest section of the oxide coating after current start ($t = 0$). Operating temperature of the cathode 730° C; emission current I_{em} and contact resistance R are parameters.*

Acknowledgments

This paper is based on investigations which the author carried out as a member of the staff of the Valve Laboratory of the Wernerwerk für Funkgerät der Siemens & Halske AG in Berlin. Thanks are due to Dir. Dr. W. Jacobi, on whose behalf the work was done, for permission to publish, and to the author's wife for linguistic supervision of the text.

REFERENCES

[1] R. Holm, "Die technische Physik der elektrischen Kontakte," Springer, 1941.
[2] W. Meyer and A. Schmidt, "Leitfähigkeit von BaO," *Zeitschr. f. techn. Physik.*, Vol. 13, p. 137 (1932).
[3] M. Benjamin, R. J. Huck and R. O. Jenkins, "Oxide Coated Cathodes," *Proc. phys. Soc.*, Vol. 50, p. 345, (1938).
[4] D. D. Knowles and J. W. McNall, "Sparking of Oxide coated Cathodes in Mercury Vapour," *J. appl. Phys.*, Vol. 12, p. 149 (1941).
[5] H. P. Fink and Körner, "Messungen des zeitlichen Verlaufes der Erwärmung in einem Kontakt infolge eines plötzlich einsetzenden Stromes," *Wiss. Veröff., Siemenswerk*, Vol. 19, p. 280, (1940).
[6] E. Patai and Z. Tomaschek, "Herstellung von Oxydschichten kolloidaler Form," *Kolloid. Zeitsch.*, Vol. 74, p. 253 (1936). P. Clausing and J. B. Ludwig, "Emissionsfähigkeit von Oxydschichten," *Physica* Vol. 13, p. 193 (1933).
[7] Landolt-Börnstein, Ergänzungsband, S.2263.
[8] W. Wien and F. Harms, "Handbuch der Experimentalphysik," Vol. 13, p. 2, Teil.
[9] A. C. Claassen and C. F. Veenemans, "Dampfdrucke von BaO SrO und CaO," *Z. f. Phys.*, Vol. 80, p. 342 (1933).
[10] E. E. Schuhmacher," Schmelzpunkte von CaO, SrO und BaO," *J. Am. Chem. Soc.*, Vol. 49, p. 396 (1936).

PUSH-PULL A.F. AMPLIFIERS

Load Curves for Classes A, B and C Conditions

By K. R. Sturley, Ph.D., M.I.E.E.

(Head of Engineering Training Department, British Broadcasting Corporation.)

SUMMARY.—Problems of the position of the composite load line and the construction of the valve load curves for classes A, B and C audio-frequency push-pull amplifiers are discussed and it is shown that B. J. Thompson's original work on class B amplifiers with matched valves can be extended to cover all classes of push-pull amplification under matched or unmatched conditions. Deductions regarding composite and valve-load curves as a result of voltage and current measurements are confirmed by photographs of valve-load curves obtained on the screen of a cathode-ray tube.

Introduction

IN an experiment requiring the symmetrical pulse-shaped waveform of Fig. 1, the author used a push-pull audio-frequency amplifier operated under Class C conditions, and during this work the question of representing graphically the operation of the valves was raised. In the subsequent investigation some interesting facts were discovered about class C push-pull operation and also about the asymmetrical operation of push-pull stages, such as occurs if one valve is operating in class C and the other in class B. Thompson[1] has already shown how class B symmetrical push-pull operation can be represented graphically. This he did by inverting the I_aV_a characteristic of one valve and by reversing the direction of its V_a axis. The voltage points corresponding to the h.t. voltage, $V_{a(b)}$, were registered together and composite IV_a characteristics were obtained by adding the appropriate I_aV_a curves. Thus if the common bias voltage was $-A$, curves of $V_g = -A \pm x$ for valve 1 were added to those of $V_g = -A \mp x$ for valve 2. A load line was drawn across the composite characteristics to pass through the point $V = V_{a(b)}$, $I = I_{01} - I_{02}$ where I_{01} and I_{02} were the quiescent anode currents of V_1 and V_2. The composite load resistance was taken to be the equivalent load resistance between one anode and the centre tap of the output transformer primary.

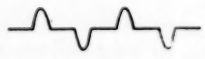

Fig. 1 (above). *Desired pulse waveform.*

Fig. 2 (right). *Circuit diagram of test apparatus.*

MS accepted by the Editor, November 1948

Thompson's article does not indicate how asymmetrical operation of push-pull valves in any combination of class A, B or C conditions can be represented on the I_aV_a curves of the valves. Furthermore, the possible relationship between the operating direct currents of each valve and the steady anode voltages is not discussed, neither is it clear whether the operating direct anode current values are more, or less, important than the quiescent (zero signal) d.c. values.

The investigation to find an answer to these questions was conveniently divided into three parts as follows :

1. Equal input signals were applied to both valves. One valve was biased to class C, and the bias of the other was varied from complete cut-off through class C to B.

2. Equal input signals were applied to both valves. One valve operated in class A and the other was varied from the class C to the class A condition.

3. The input voltage to one valve operating in class A was fixed and the input voltage to the other, set for class B, was varied.

Test Apparatus and Procedure

A circuit diagram showing values of components for the test apparatus is shown in Fig. 2. The slide-back diode voltmeter was used to measure the maximum and minimum voltages on valves V_1 and V_2. After preliminary tests it was only necessary to measure voltages on one valve, since it was found that coupling between both halves of transformer primary was very nearly unity.

I_aV_a characteristics were obtained for both valves and those for V_2 were inverted and reversed as suggested by Thompson. The composite load line ($\frac{1}{4}R = 9975\ \Omega$) was drawn across these characteristics through a point $V_a = V_{a(b)}$, $I = I_{av1} - I_{av2}$, where I_{av1} and I_{av2} were the operating (not quiescent values, which were zero) direct currents of each valve. The maximum and minimum anode voltages read by the diode were used as the terminating points of the load lines.

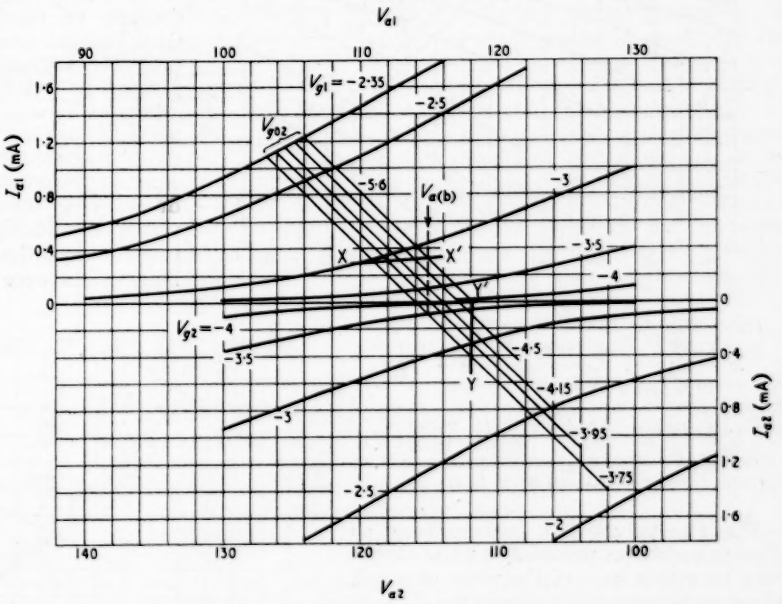

Fig. 3. *Load lines for Test 1; $V_{a(b)} = 115$ V, $V_{g01} = -4$ V, $V_{g02} = -5.6$ to -3.75 V, $E_{s1} = E_{s2} = 1.65$ V peak.*

Test 1. Both Valves in Class C.

The results of this test are shown in Fig. 3. The locus of the extremities of the load lines set by the minimum and maximum anode voltages all lie on their correct grid bias lines; e.g., the locus of the maximum I_{a1} ends of the lines falls on the curve for $V_{g1} = -2.35\text{V} = -4$ (fixed bias) + 1.65 (peak input signal). This is to be expected since only one valve is conducting at a time. It also confirms that the operating, and not quiescent, direct anode currents determine the location of the load line. Curves XX' and YY' are the loci of the direct anode currents.

Fig. 3 shows that the operation of each valve is identical to that of a valve having a d.c. load resistance $R/4$ and a variable h.t. voltage equal to the intercept of the load line with the V_a axis. If the average voltage component ($I_{av1}\,R/4$) of the pulse on V_1 is subtracted from that ($I_{av2}\,R/4$) of the pulse on V_2, and the resultant voltage added to the load line intercept voltage (the equivalent h.t.), $V_{a(b)}$, is obtained. This, therefore, indicates the relationship between the operating direct anode currents and the steady anode voltage, in this instance the h.t. voltage, $V_{a(b)}$.

Test 2. Valve V_1 in Class A and V_2 varying from Class C to A.

Fig. 4 shows the result of drawing the load lines across the I_aV_a curves in the manner outlined in Test 1. The V_1 extremities of the load lines start on the $V_{g1} = -1.35$ volts curve when V_2 is in class C but depart from this curve as V_2 approaches the class A condition. The departure is due to V_2 becoming conductive, for example, the lowest load line has a peak anode current value of 3.3 mA at its extremity where $V_{a1} = 112$. Since the instantaneous grid bias

of V_2 for this condition is $(-3.12-1.65)$ -4.77 V, it has an anode current of 0.35 mA which when added to the 3.3 mA of the composite line gives the current on the $V_{g1} = -1.35$ V curve at $V_{a1} = 112$ V.

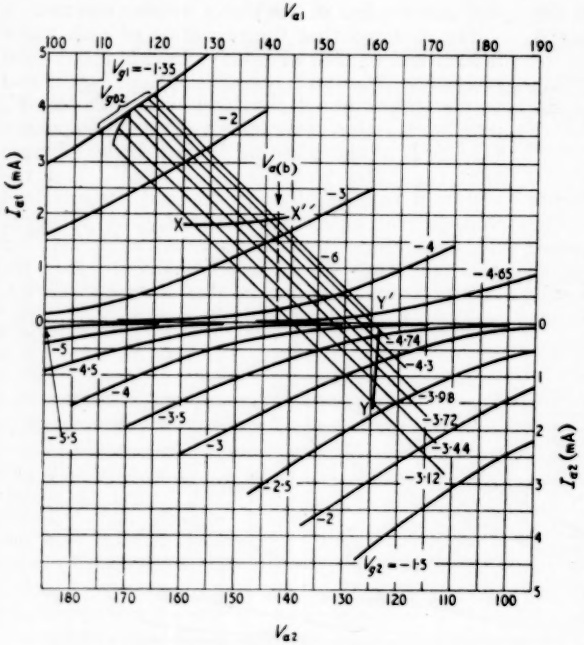

Fig. 4 (above). *Load lines for Test 2;* $V_{a(b)} = 142.5$ V, $V_{g01} = -3$ V, $V_{g02} = -6$ *to* -3.12 V, $E_{s1} = E_{s2} = 1.65$ V *peak. Locus of* $I_{av1} - XX'$; *locus of* $I_{av2} - YY'$.

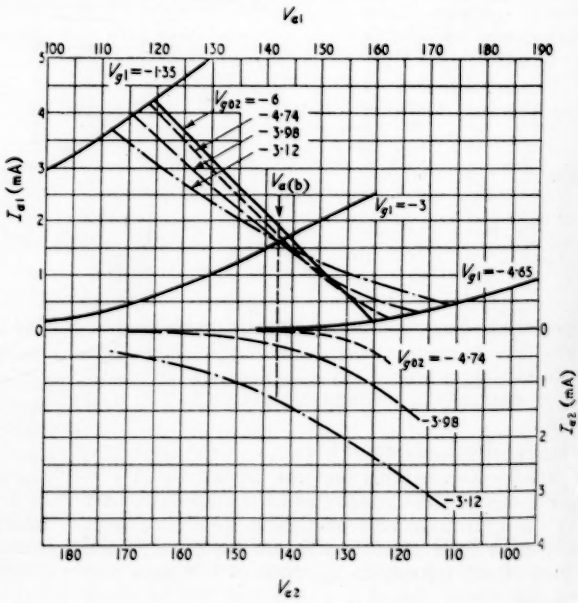

Fig. 5 (right). *Load curves for valves* V_1 *and* V_2 *for Test 2;* $V_{a(b)} = 142.5$ V, $V_{g01} = -3$ V, $V_{g02} = -6$ *to* $= 3.12$ V, $E_{s1} = E_{s2} = 1.65$ V *peak.*

The two valves may be considered as though each were providing a pulse of current on either side of the point at which the composite load line crosses the V_a axis, and the conclusions regarding operating direct anode currents, average voltage components of each pulse and the steady anode voltage, $V_{a(b)}$, are as set out in the first test. In actual fact the valve load curves themselves are not coincident with the composite load curves, and the former may be found by following the procedure established by Thompson; viz, by first constructing the composite IV_a curves and projecting vertically from the intercepts between them and the load line on to the appropriate valve bias curves. Since the valves are asymmetrical a composite curve is formed by adding valve V_1 curves for $V_{g01} \pm x$ to those of V_2 for $V_{g02} \mp x$. The result of doing this is shown in Fig. 5 for four selected values of V_{g02} and it is interesting to note that harmonic distortion in one valve due to 'bottom bending' can be reduced by using another valve operating in class C in push-pull relationship to the first.

The curves for valve V_1 in Fig. 5 show that when both valves are operating over the complete cycle and producing almost equal positive and negative anode voltage swings the valve load curves pass through the quiescent anode current point at $V_a = V_{a(b)}$. When one valve is cut off during part of the cycle, the load curve of the fully conducting valve passes through an anode-current point greater than the quiescent value. This suggests that the load curve of V_1 changes its position as well as length when the signal inputs of V_1 and V_2 are varied and V_2 is partially conducting, but pivots through the quiescent point, when both valves conduct continuously. This was confirmed by varying the equal input signals to valves V_1 and V_2; the change in operating-current difference was negligible when both valves were fully conducting.

Test 3. Valve V_1 in Class A and Valve V_2 in Class B with Input Signal Variation.

The results, indicated in Fig. 6, show that the locus of the V_1 extremities of the load lines follow the $V_{g1} = -1.4$ V $(-3 + 1.6)$ curve only when the peak input signal to V_2 exceeds about 1.25 volts. For peak signal values less than this, valve V_2 is conducting and if its anode current

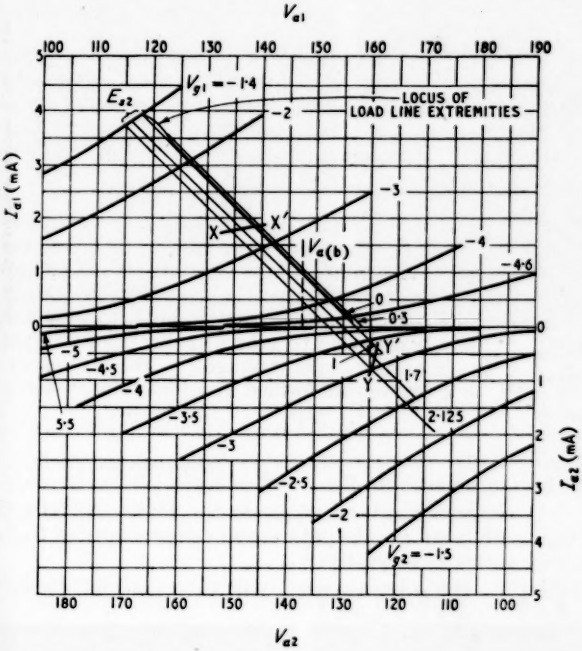

Fig. 6. *Load lines for Test 3;* $V_{a(b)} = 142.5$ V, $V_{g01} = -3$ V, $V_{g02} = -4$ V, $E_{s1} = 1.6$ V *peak*, $E_{s2} = 0$ *to* 2.125 V *peak*.

at the particular value of $V_{a1\,(min)}$ is added to that of the composite line, the resultant current point lies on the $V_{g1} = -1.4$ V curve. Composite IV_a curves may be obtained by adding curves of $V_{g2} = -3 \pm x$ to curves of $V_{g2} = -4 \mp x\,E_{s2}/E_{s1}$ where E_{s1} and E_{s2} are the peak input signals to V_1 and V_2. The valve load curves may then be derived as in Test 2 and the result for four selected E_{s2} values is shown in Fig. 7. At $E_{s2} = 0$, the anode currents registered by the $V_{g2} = -4$ V curve at the particular values of $V_{a1\,(min)}$ must be added to the appropriate currents of the composite load line in order to obtain the load curve for valve V_1. The result is a steeper curve and this is to be expected because the slope resistance of V_2 is acting in parallel with $R/4$. The load curve for V_2 is the $V_{g2} = -4$ V curve. As E_{s2} is increased the direct anode current of V_2 falls to a minimum at $E_{s2} = 0.5$ and then increases; at the same time the slope of the V_2 load curve changes.

It was noted in all the above tests that if a direct anode current reading of valve V_1 was taken with V_2 removed and vice versa the difference between these current values was practically the same as the current difference with the valves operating together, and measurements on each valve alone could be used to determine the position of the composite load line.

Test 4. Confirmatory Check using a C.R. Oscilloscope.

To check the method of obtaining the valve load curves, the circuit of Fig. 2 was slightly modified to permit the valve load curves to be delineated on a cathode-ray tube screen. The two milliammeters (mA) in Fig. 2 were replaced by 100-Ω resistors and the capacitors C_1 were removed. The input to the push-pull d.c. amplifier supplying the y-plates of the c.r. tube was derived from the 100-Ω resistor in the cathode of V_1 or V_2; the input to the x-amplifier was connected to the anode of V_1 or V_2 through a 'back-balancing' battery neutralizing $V_{a(b)}$.

Photographs of the c.r. tube traces for the three test conditions are shown in Figs. 8(a) and (b), 9 and 10(a) and (b). The load curves of V_2 were inverted and reversed before printing on the same sheet as those for V_1, and, in order to avoid confusion, a space is left between the x-axes which were otherwise correctly registered. These axes were traced by short-circuiting the input to the y-amplifier. Scale divisions across the traces are due to a scale engraved on the face of the c.r. tube.

It is clear from Fig. 8(a) that the valve-load curves are straight lines corresponding to the resistance load and are parts of the same composite load line. In Fig. 8(b) load lines for V_1 only are shown; the gain of the y-amplifier was increased in order to show the decrease in peak anode current as the extremities of the load lines follow the $V_{g1} = -2.35$-V bias curve.

Fig. 9 is the equivalent of Fig. 5. The change in shape of the V_1 load curve from the straight line when V_2 is inoperative and the upwards travel of the $I_{a1\,(min)}$ extremity of the load curve along the $V_{g1} = -4.65$-V curve are clearly illustrated. The $I_{a1\,(max)}$ extremities of the V_1 load curves show a more marked fall than those of Fig. 8(b) because their locus is a much lower

V_{g1} bias curve (— 1.35 instead of — 2.35 V).

The similarity between Fig. 10(a) and Fig. 7 is marked and the reversal of the slope of the V_2 load curve as E_{s2} is increased is very noticeable.

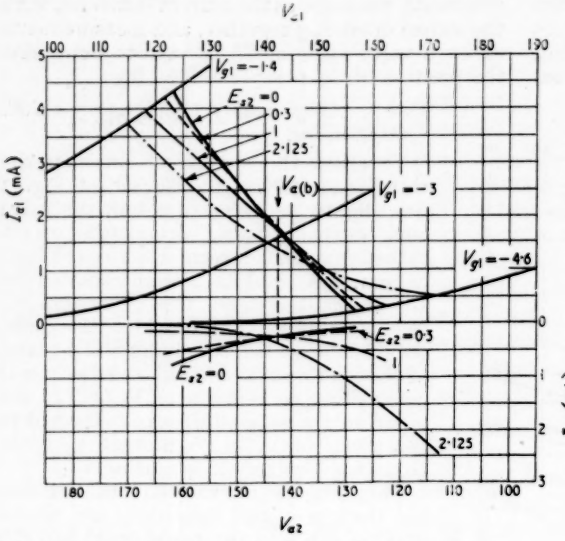

Fig. 7. *Load curves for valves* V_1 *and* V_2 *for Test* 3 *;* $V_{a(b)} = 142.5$ V, $V_{g01} = -3$ V, $V_{g02} = -4$ V, $E_{s1} = 1.6$ V *peak*, $E_{s2} = 0$ *to* 2.125 V *peak*.

The effect on the load curve of V_1 if V_2 is removed when E_{s2} is zero is illustrated in Fig. 10(b). The bottom load line of lower slope is the line due to the resistance $R/4$ alone and the top one shows the additional load thrown in to V_1 by V_2.

These photographs confirm the method of obtaining the valve load lines.

Conclusions

The important conclusions to be drawn from this investigation are :—

(1) The location of the composite load line at $V_a = V_{a(b)}$ is determined by the difference between the operating currents and not the quiescent currents of the push-pull valves.

(2) The difference between the operating currents for either valve working alone under given conditions is very nearly equal to the difference between the operating currents of the valves working in push-pull under the same conditions. This means that the current difference of the valves operating singly can be used to locate the position of the composite load line.

(3) In any type of push-pull circuit the valves may be considered as though each provides a pulse of current and voltage on either side of the point V_a (read on the V_{a1} axis) at which the composite load line cuts the V_a axis. The average voltage of each pulse is the product of the operating direct anode current and the composite load resistance; if for valves V_1 and V_2 these are V_{av1} and V_{av2}, then they and V_a' are related to the h.t. voltage $V_{a(b)}$ by the following expression :

$$V'_a + V_{av2} - V_{av1} = V_{a(b)}$$

(4) Thompson's method of obtaining IV_a characteristics and, from these, of determining the performance of matched push-pull valves is proved to be correct and capable of extension to unmatched valves and to valves having unequal input and/or bias voltages. The composite curves are formed by adding bias curves of

$$V_{g1} = V_{g01} \pm x \text{ (valve } V_1\text{) to}$$

$$V_{g2} = V_{g02} \mp \frac{E_{s2}}{E_{s1}} x \text{ (valve } V_2\text{)}$$

where V_{g01} and V_{g02} are the bias voltages and E_{s1} and E_{s2} the peak signal voltages applied to V_1 and V_2 respectively.

(5) When the push-pull valves are matched or nearly matched, the valve load curves pass through the quiescent anode current point at $V_a = V_{a(b)}$ and change of input signal to both valves causes the load curves to change in length only. The difference between the operating

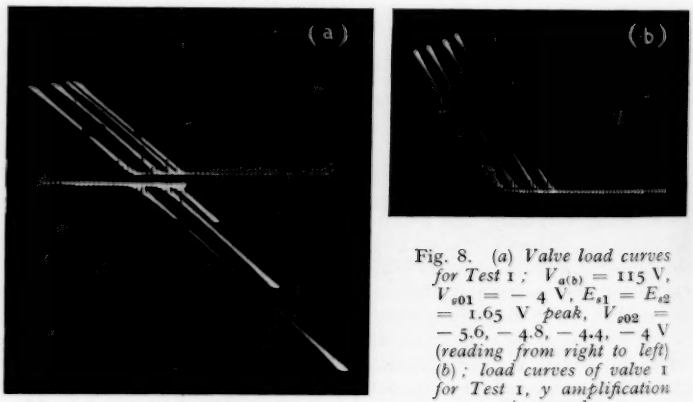

Fig. 8. (*a*) *Valve load curves for Test* 1 *;* $V_{a(b)} = 115$ V, $V_{g01} = -4$ V, $E_{s1} = E_{s2} = 1.65$ V *peak*, $V_{g02} = -5.6, -4.8, -4.4, -4$ V *(reading from right to left)* (*b*) *; load curves of valve* 1 *for Test* 1, *y amplification increased.*

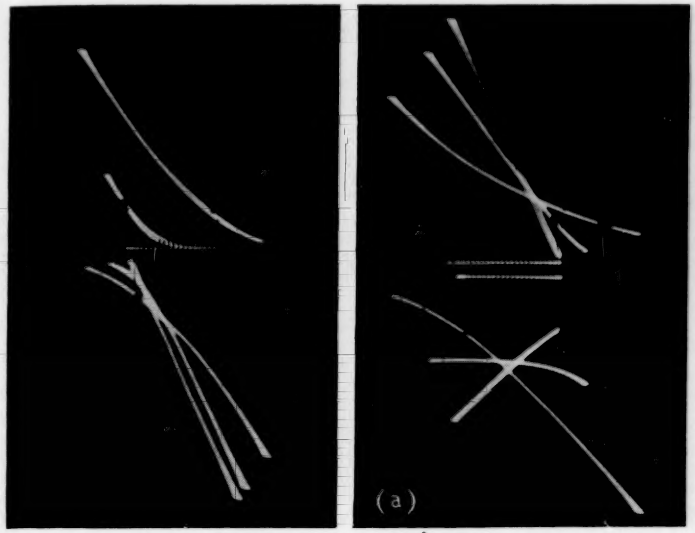

Fig. 9 (left). *Valve load curves for Test 2,* $V_{a(b)} = 142.5$ V, $V_{g01} = -3$ V, $E_{s1} = E_{s2} = 1.65$ V *peak,* $V_{g02} = -6, -4.2, -3$ V *(reading from right to left at top).*

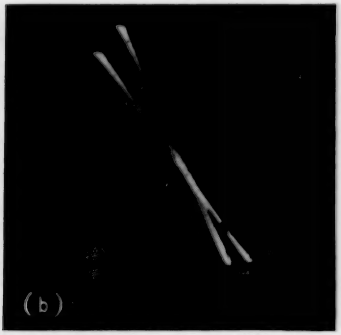

Fig. 10. *(a) Valve load curves for Test 3,* $V_{a(b)} = 142.5$ V, $V_{g01} = -3$ V, $V_{g02} = -4$ V, $E_{s1} = 1.6$ V *peak,* $E_{s2} = 0, 1, 2.125$ V *peak (reading from right to left at top). (b) load curve for valve* V_1, $E_{s2} = 0$ V; *lower slope line* V_2 *removed, higher slope line* V_2 *operative.*

currents is almost independent of input signal variation and is equal to the quiescent difference.

If the valves are not matched both composite and valve load curves tend to change position as well as length when the input signals to both valves are varied together.

Acknowledgment

The author desires to record his indebtedness to A. E. Robertson for photographing and printing the c.r. tube traces.

REFERENCE

[1] B. J. Thompson. "Graphical Determination of Push-Pull Audio Amplifiers." *Proc. Inst. Radio Engrs,* Vol. 21, No. 4 (April 1933) p. 591.

BOOK REVIEW

Radio-Frequency Heating Equipment

By L. L. LANGTON, A.M.I.E.E. Pp. 196+IX. Sir Isaac Pitman & Sons, Ltd., Parker St., Kingsway, London, W.C.2. Price 17s. 6d.

This book deals with both dielectric and eddy-current heating and, after opening chapters describing the properties of the materials to be heated, thermionic power generators are treated. Methods of coupling the generator output to the work circuit for both types of heating are dealt with. Subsequent chapters cover properties of valves and power-supply systems, and the two concluding chapters deal with applications.

It is a little difficult to discover for whom the book is intended. In his preface, the author says that his object " is to deal mainly with the generation and transfer of Radio-frequency Power, in a manner suited to the needs of those having an interest in Radio-frequency Heating." The nature of this interest is not stated. The non-technical user of the apparatus is unlikely to find the book helpful, for it consists mainly of a mixture of design equations and physical descriptions of the mode of operation which would not be very intelligible to him. The equipment designer, on the other hand, is likely to need a much more thorough treatment, although he will find a good deal of use to him in this book.

The difficulties of the reader are not helped by the confusing and undefined nomenclature adopted. In the introductory chapter the word ' charge ' is used for the material to be heated, but in Ch. 2 ' charge ' becomes electrical charge and the material to be heated becomes the ' work.' This term ' work ' is the one most used in the book, but nevertheless it becomes ' charge ' at intervals and for no apparent reason. This is very confusing and the use of the word should be confined to electrical charge.

The author's use of ' blocking ' to describe the condition which occurs in a valve oscillator when reverse grid current locks the grid positive is to be deprecated. This term is properly used to describe just the opposite condition—that in which the grid becomes so negative that both grid and anode currents are cut-off and the valve is blocked. The positive-grid condition is known by some as ' locking ' but this word is too easily confused with ' blocking ' for it to be really satisfactory.

Much of the book is taken up with the difficulties of keeping a proper load on the generator and of transferring the power to the work. The difficulties are accentuated by some confusion in the usage of 'load', for it sometimes means power and sometimes resistance !

The mathematics employed are essentially simple ; but many of the formulae are only approximations and must be used with caution. The equations, especially in Appendix I, are not always free from errors.

W. T. C.

CORRESPONDENCE

Letters to the Editor on technical subjects are always welcome. In publishing such communications the Editors do not necessarily endorse any technical or general statements which they may contain.

Maxwell's Theory and Relativity

SIR,—Professor Howe's Editorial in the July *Wireless Engineer*, and my letter in the same issue, bring us to a measure of agreement about the problem of the e.m.f. induced in a coil by an electric charge in uniform relative motion. That is, we agree that, when the acting charge is stationary and the coil moving, the motion of the charges induced on the coil by the stationary acting charge causes, by Maxwell's theory, a magnetic field which induces in the coil the same e.m.f. as is induced when the coil is stationary and the acting charge is moving.

Since, however, Professor Howe does not deal with the other implications of the problem indicated in my letter, he gives me the impression that the problem is now solved to his satisfaction and that he also regards Maxwell's theory as being fully capable of dealing with all possible cases. With this view I am unable to agree. In my letter I formulated a problem involving two insulating discs on the peripheries of which are situated equally-spaced and equally-charged conducting segments, these being positively charged on one disc and negatively charged on the other. If these discs are situated close together on the same stationary axis and an electric charge moves by, then by Maxwell's theory the two discs should experience opposite torques and, if allowed to rotate, their rotation will be equivalent to the circulation of a current around a circular loop. When, however, the acting charge is stationary and the discs move, no torque is forecast by Maxwell's theory, and the inconsistency can be resolved only by using Einstein's ' restricted ' theory of relativity.

Lest it be objected that this is an electro-mechanical problem rather than an electromagnetic one, let us consider the following.

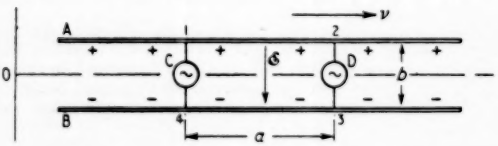

Fig. 1

In Fig. 1, A and B are the conducting plates of a parallel-plate capacitor, assumed to be large enough to make the electric field between them uniform in the region to be considered. C and D are two identical alternators whose e.m.fs are in phase, distant a apart and charging the capacitor in parallel. Suppose that the plates are rectangular, being long in proportion to their breadth, and that the alternators are connected to points on the centre lines of the plates, so that the whole arrangement has symmetry. Then clearly, if the alternator e.m.fs are equal and in phase, no circulating current is set up around the closed conducting path 1-2-3-4.

Now let the whole arrangement move from left to right with uniform velocity v. Since the plates are electrostatically charged this motion will cause a magnetic field perpendicular to the paper and linking the circuit 1-2-3-4. Further, since the p.d. between the plates is alternating, this magnetic field will alternate also. Since its value is the same at each alternator, no net e.m.f. will be induced around the circuit by the motion of the connecting wires 1-4 and 2-3 through the field, but *an e.m.f. will be induced owing to the changing linking flux*.

Let us calculate this e.m.f. If each alternator has an e.m.f. equal to $E_m \sin \omega t$, then the electrostatic field between the plates, neglecting resistance and inductance, will be :

$$\mathfrak{E} = \frac{E_m}{b} \sin \omega t \quad .. \quad .. \quad .. \quad .. \quad .. \quad (1)$$

The motion of this field (i.e., of the charges which cause it) with velocity v sets up a magnetic field given by :

$$B = \frac{v\mathfrak{E}}{c^2} = \frac{vE_m}{bc^2} \sin \omega t \quad .. \quad .. \quad .. \quad .. \quad (2)$$

which will be perpendicularly down into the paper when the plate A is positive. The flux linking the circuit 1-2-3-4 is therefore :

$$\phi = abB = \frac{vaE_m}{c^2} \sin \omega t \quad .. \quad .. \quad .. \quad (3)$$

so that the e.m.f. is given by :

$$e_m = -\frac{d\phi}{dt} = -\frac{va\omega E_m}{c^2} \cos \omega t \quad .. \quad .. \quad (4)$$

Fig. 2

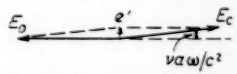

Fig. 3

Taking a clockwise e.m.f. as positive, the vector diagram, with r.m.s. values, is as shown in Fig. 2. Thus a net e.m.f. exists around the circuit whose value is directly proportional to the velocity of translation v relative to the observer.

This is obviously an absurd result, but appears to be what Maxwell's theory predicts.

Let us now see how this absurdity is removed by the Theory of Relativity. Take the origin of the observer's frame of reference at o (Fig. 1) and the motion along the x-axis. Consider the instant when the alternator C is distant x from o. Then the theory of relativity tells us that, if t_0 is the ' local ' time at o, the local time at the *moving* alternator C is :

$$t_C = \beta \left(t_0 - \frac{vx}{c^2} \right) \quad .. \quad .. \quad .. \quad .. \quad .. \quad (5)$$

and that the local time at the moving alternator D is :

$$t_D = \beta \left(t_0 - \frac{v(x + a)}{c^2} \right) \quad .. \quad .. \quad .. \quad .. \quad (6)$$

where $\beta = (1 - v^2/c^2)^{-\frac{1}{2}}$, which may be put equal to unity for laboratory values of v*

Hence there is a *difference* of ' local ' time between the two alternators given by :

$$t_C - t_D = \frac{va}{c^2} \quad .. \quad .. \quad .. \quad .. \quad .. \quad (7)$$

which means that if two clocks are placed at C and D

* The length a is also shortened to a/β and the field $\mathfrak{E}$ increased to $\beta\mathfrak{E}$ in the stationary reference system. Thus the flux ϕ is unaffected.

and synchronized when the arrangement is stationary, when moving the clock at C will indicate a time va/c^2 *ahead* of that at D.

Thus, although the two alternators were in synchronism when stationary, they are no longer so when moving. A time advance in phase of C with respect to D of amount va/c^2 corresponds to a leading phase angle of $va\omega/c^2$ radians. This is illustrated in the vector diagram of Fig. 3. Thus the vector sum of E_C and E_D is no longer zero, but is given by :

$$e' = 2E \sin \frac{va\omega}{2c^2} = \frac{va\omega E}{c^2} \quad .. \quad .. \quad .. \quad (8)$$

leading E_C by $\pi/2$, since the phase angle $va\omega/c^2$ is very small.

Clearly e' exactly cancels the e.m.f., given by (4), induced by the alternating magnetic field, so that the resultant e.m.f. in the circuit comes out to be zero, as when the apparatus is stationary.

We therefore have a case in which an alternating linking flux definitely exists according to Maxwell's theory, but in which the resultant e.m.f. is zero. It seems that the calculation of second-order e.m.fs in moving circuits is not as simple as at first appears. It may therefore be expected, as I suggested in my letter in the July issue, that proper application of the theory of relativity will remove the e.m.f. due to the magnetic effect of the induced surface charges in the case of moving coil, stationary charge, and will also reinstate the acting charge as the direct inducer of the required e.m.f.

This example, I think, definitely shows that Maxwell's theory is by itself not always consistent with the principle of relative motion. When it is consistent, as in the case of a moving conducting magnet and the problem of the coil and charge, the consistency is due to the particular electrical properties of conductors, a happy accident which nevertheless appears to have been the cause of a considerable amount of confusion.

Dundee. E. G. CULLWICK.

Circular-Ring Filters in Round Waveguide

SIR,—A resonant circular metal ring (with a periphery slightly greater than the free-space wavelength) is an effective filter for the TE_{11}-mode in a circular waveguide. It would seem that the effectiveness must be increased by placing two filters at a distance of $\lambda_g/4$ (λ_g is the wavelength in the waveguide). We have found that this is not the case ; i.e., the transmission coefficient of the two filters $\lambda_g/4$ apart is not sensibly lower than the coefficient of the single filter. On increasing their separation, however, the transmission coefficient decreases, and has a minimum between $\lambda_g/4$ and $\lambda_g/2$ and a maximum at $\lambda_g/2$. Beyond this the shape of the curve is normal with large minima at $3\lambda_g/4$, $5\lambda_g/4$, etc.

This phenomenon can be explained by supposing that a coupling exists between the two filters when they are separated by less than $\lambda_g/2$. This coupling occurs in the TE_{11} and higher-modes. The effect becomes accentuated when the wavelength is decreased.

When the first of the two filters is in resonance, we can obtain very simply the characteristics of a second filter by measuring the separations of the two filters for the position of maximum transmission coefficient. If in this position the difference in their separation from $\lambda_g/2$ is Δl, the angle of the reflection coefficient is $\phi = 4\pi \frac{\Delta l}{\lambda_g}$ $+\pi$, its absolute value is : cos ϕ and the impedance of the filter is $Z = -\frac{1}{2} \tan \phi \, Z_c j$. This method of measuring the characteristics of obstacles is easier than by the s.w.r. method and it is necessary to measure distances only.

ZOLTAN SZEPESI.

Laboratoire de Haute Fréquence de la Faculté des Sciences, Grenoble, France.

Spontaneous Fluctuations in Double-cathode Valves

SIR,—D. K. C. MacDonald[1] published in your journal measurements on the fluctuation temperature of a directly-heated double-cathode valve, which indicated that for filament temperatures higher than about 2,000° K the ratio β of fluctuation temperature to true temperature increases rapidly with temperature.

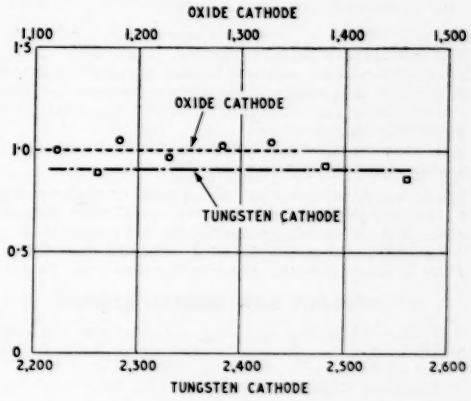

We have carried out analogous measurements at a frequency of 6 Mc/s on a valve consisting of two indirectly-heated plane cathodes 1 mm apart and with surfaces of 1.5 × 0.4 cm² as well as on a valve with two directly-heated tungsten filaments of 100-μ diameter, 2-cm length and 0.5 mm apart (in both cases for different cathode temperatures). The results of our measurements are shown in the figure. With the indirectly-heated cathodes the temperature was varied from 1,100° to 1,330° K. The circles denote the values of β. The temperature range for the directly-heated filaments extended from 2,260° to 2,560°. The squares give the values of β. It may be concluded that within the limit of experimental error nowhere in this wide range is found a value of β higher than 1. The values obtained for the directly-heated valve are somewhat lower than 1. This may be caused by the presence of a cold glass wall which, although at a comparatively great distance, may influence the space charge and movement of electrons within the valve.

We conclude that our measurements cannot give any support to the theory of Fürth[2] from which values of β higher than 1 could be expected.

We, therefore, agree with MacDonald's second article[3] in which he criticizes Fürth's theory.

K. S. KNOL
G. DIEMER

Philips Research Laboratories, Eindhoven, Holland.

REFERENCES

[1] Mac Donald, D.K.C., *Wireless Engr*, Vol. 24, p. 30, 1947.
[2] Fürth, R., *Proc. roy Soc.*, A. Vol. 192, p. 593, 1948.
[3] Mac Donald, D.K.C., *Proc. roy. Soc.*, A. Vol. 195, p. 225, 1948.

WIRELESS PATENTS

A Summary of Recently Accepted Specifications

The following abstracts are prepared, with the permission of the Controller of H.M. Stationery Office, from Specifications obtainable at the Patent Office, 25, Southampton Buildings, London, W.C.2, price 2/- each.

ACOUSTICS AND AUDIO-FREQUENCY CIRCUITS AND APPARATUS

621 032.—A sound amplifier or reproducer including a closed chamber with a diaphragm to which air is supplied under pressure, the air flow being controlled by a voice coil.

Charles Franklin Dilks. Convention date (U.S.A.) 28th May, 1941.

622 241.—Ribbon type pick-ups having two side-by-side conductors passing through a magnetic field and interconnected at one end: said conductors are fixed at one end and at the other they are rocked by a stylus carrier including a highly resilient material of high molecular friction.

Truvox Engineering Company Limited and Frederick Clark. Application date 10th September, 1946.

622 830.—A capacitance microphone or pick-up feeding a cathode-follower circuit with particular means for obtaining a polarizing potential for the microphone.

P.R.T. Laboratories Limited, Bernard Jay Solley and Peter William Roberts. Application date 22nd July, 1946.

AERIALS AND AERIAL SYSTEMS

615 722.—Inductive coupling arrangement between an aerial and a single-wire transmission line, the latter being an integral number of quarter-waves long.

Standard Telephones and Cables Ltd. and E. O. Willoughby. Application date 10th August, 1945.

620 773.—Elbow for rectangular waveguides having adjustable rods or screws positioned to rotate the vectors about the axis of travel.

C. W. Miller, G. J. Scoles and Metropolitan-Vickers Electrical Company Limited. Application date 21st August, 1946.

622 211.—Pick-up loop for u.h.f. particularly for a wavemeter having a C-shaped element spanned by the heating element of a thermocouple.

Submarine Signal Company. Convention date (U.S.A.) 10th March, 1945.

DIRECTIONAL AND NAVIGATIONAL SYSTEMS

614 595.—Radiolocation apparatus with a plan-position indicator in which the target is shown against a background forming a pictorial chart of the area under exploration.

G. E. Partington. Application date 16th July, 1946.

615 576.—Modulating device for reducing and stabilizing the time interval required for the building-up of trains of pulsed signals by a high-frequency oscillator, say in radiolocation.

D. H. Priest. Convention date (U.S.A.) 28th, June, 1945. [*See note on specification.*]

620 656.—Beacon modulator for producing differently characteristic signals on opposite sides of the course wherein the outputs from two signal sources are fed to balanced and unbalanced modulators with phase reversal from one source, the modulator outputs being combined by a bridge.

Standard Telephones and Cables Limited (assignees of S. B. Pickles). Convention date (U.S.A.) 26th August, 1943.

621 575.—Direction and distance finder wherein a mobile station receives a sine-modulated carrier and radiates a correspondingly modulated carrier of a different frequency with a predetermined phase relation thereto.

Standard Telephones and Cables Limited, C. W. Earp and R. F. Cleaver. Application date 21st June, 1946.

621 733.—Rotary beacon transmitter, the carrier wave of which is modulated by two different signals whose phase difference corresponds to the instantaneous position of the beam.

J. W. S. Pringle. Application date 23rd April, 1945.

621 837.—Aerial navigation device wherein the aircraft emits a scanning beam which is reflected by members set in pairs on the ground on opposite sides of the course and indicated on a c.r. tube.

Curtis Pump Company. Convention date (U.S.A.) 2nd September, 1943.

622 458.—Electronic switching device for switching several directional aerials to an amplifier and connecting thereto the corresponding windings of an indicating meter.

J. R. Steinhoff. Convention date (U.S.A.) 20th October, 1944.

RECEIVING CIRCUITS AND APPARATUS

(*See also under Television*)

613 026.—Automatic gain-control system in which the control voltage is derived from a point in the circuit of relatively-positive potential and is subject to the constant voltage drop across a glow-discharge tube.

Marconi's W.T. Co. Ltd. (assignees of G. L. Fredendall and A. C. Schroeder). Convention date (U.S.A.) 29th August, 1944.

613 099.—Permeability-tuned input circuit, combined with a main and an auxiliary frame aerial, to give a wide frequency cover.

Marconi's W.T. Co. Ltd. (assignees of V. D. Landon). Convention date (U.S.A.) 27th January, 1940.

613 152.—Tuning system wherein a given wave range is selected for band-spreading by switching one or other of a set of auxiliary inductances into circuit with a common capacitor.

Philips Lamps Ltd. Convention date (Netherlands), 1st July, 1941.

613 952.—Stabilizing the output from a limiter valve by ballasting the cathode-supply circuit, particularly in a.g.c. systems.

Philip's Lamps Ltd. Convention date (Netherlands) 6th November, 1941.

614 329.—Double-diode limiter devices, with adjustable thresholds, for reducing undesirable noise components in the reception of frequency-modulated signals.

Marconi's W.T. Co. Ltd. (assigness of M. G. Crosby). Convention date (U.S.A.) 9th December, 1944.

614 355.—Crystal-to-metal rectifier for ultra-short waves wherein the wire is arranged to make a linear, as distinct from a point contact with the crystal.

Western Electric Co. Inc. Convention date (U.S.A.) 27th July, 1945.

615 481.—Receiving cabinet fitted with two laterally-adjustable loudspeakers, for the stereophonic reproduction of sound transmitted over separate channels.
Philips Lamps Ltd. Convention date (Netherlands) 18th March, 1942.

615 536.—Receiver for frequency-modulated signals, in which the discriminating circuits are built-up of resistance and capacitance only, and are substantially free from inductance.
Marconi's W.T. Co. Ltd. (assignees of G. Jacobs). Convention date (U.S.A.) 27th October, 1944.

615 878.—Push-pull amplifier for ultra-short waves, in which a capacitive impedance is arranged between the two cathodes to reduce input damping.
Philips Lamps Ltd. Convention date (Netherlands) 12th November, 1942.

615 957.—Valveholder and socket, which also serves to support the valve screen and earth it effectively to the chassis of the radio set.
Cinch Manufacturing Corporation (assignees of S. M. Del Camp). Convention date (U.S.A.) 7th November, 1942.

615 987.—Reflex amplifier circuit in which negative reaction is used in order to increase the effect of automatic gain control.
Philips Lamps Ltd. Convention date (Belgium) 3rd March, 1945.

616 000.—Detector arrangement for microwaves, comprising an absorption gas contained in a cavity resonator which is coupled to a piezo-electric crystal.
Marconi's W.T. Co. Ltd. (assignees of W. D. Hershberger). Convention dat. (U.S.A.) 28th May, 1945.

616 013.—Circuit device for preventing microphonic interaction between the loudspeaker and one or other of the tuning capacitors of a radio set.
Philips Lamps Ltd. Convention date (Netherlands) 13th November, 1942.

615 468.—Mounting and illumination of a vertical rectangular-shaped tuning dial on the cabinet of a radio receiver.
Philips Lamps Ltd. Convention date (Netherlands) 17th January, 1942.

616 045.—Shunt device for preventing the distortion that normally occurs when a frequency-modulated carrier wave is passed through a tuned circuit.
Philips Lamps Ltd. Convention date (Netherlands) 13th November, 1942.

616 065.—Construction of a sealed-in crystal point-contact rectifier for detecting, or mixing, ultra-short waves.
The General Electric Co. Ltd., and R. W. Douglas. Application date 23rd August, 1946.

TELEVISION CIRCUITS AND APPARATUS

FOR TRANSMISSION AND RECEPTION

612 730.—Combined sound-and-picture transmission system, using a common carrier wave, or channel, and a switching-device, for illustrating a lecture with a series of still pictures.
Scophony Ltd. and G. Wikkenhauser. Application date 28th March, 1946.

613 857.—Gating device for receiving television signals of the type in which the audio component is radiated by modulating the width of the line-synchronizing pulses.
E. L. C. White. Application date 26th January, 1946.

613 877.—Multi-channel signalling systems for the transmission of wide-band signals, particularly three-colour television, with a high signal/noise ratio.
Standard Telephones and Cables Ltd. and K. G. Hodgson. Application date 20th May, 1946.

614 560.—Circuit network, including a valve, capable of assuming two different values of resistance, for discriminating between long and short pulses, say in television scanning.
R. F. Equipment Ltd. and A. W. Keen. Application date 6th June, 1946.

614 691.—Signal-level control device for maintaining a correct ratio between the d.c. 'background' component and the video signals, in the power amplifier of a television transmitter.
Farnsworth Television and Radio Corporation. Convention date (U.S.A.) 25th October, 1945.

614 942.—Television transmitter in which auxiliary pulsed signals are applied to the video-modulated carrier, in order to prepare pedestals or datum-lines for the synchronizing signals.
La "Radio-Industrie" S.A. Convention date (France) 23rd August, 1945.

615 207.—Television transmitter in which some of the energy normally lost in the power amplifier is recovered and applied to augment the original signal.
W. W. Triggs (communicated by Farnsworth Television and Radio Corporation). Application date 6th February, 1945.

615 614.—Optical system and scanning sequence for the reproduction of televised pictures in natural colours.
The General Electric Co. Ltd. and L. C. Jesty. Application date 12th June, 1944.

615 638.—Switching-device, interlocked with the normal scanning-system, for changing over from one television camera to another, without producing unsightly 'splashes.'
E. L. C. White. Application date 15th January, 1946.

615 660.—Device for eliminating spurious signals from the re-insertion network used in a television receiver to restore the d.c. component lost in transmission.
Marconi's W. T. Co. Ltd. (assignees of A. V. Bedford). Convention date (U.S.A.) 17th March, 1945.

TRANSMITTING CIRCUITS AND APPARATUS

(*See also under Television*)

612 967.—System for distributing police or military messages to a series of mobile receivers, through repeater stations operating on frequencies that are slightly different from that of the master station.
Marconi's W. T. Co. Ltd. and J. E. H. Welply. Application date 11th June, 1946.

613 217.—Combined transmitter and receiver designed for two-way operation on the same carrier wave, which can be varied over a given frequency range.
S. G. Dehn (communicated by Collins Radio Co.). Application date 6th June, 1946.

613 624.—Combined transmitter and receiver for two-way operation on the same carrier wave, including a local heterodyne unit of fixed and variable oscillators.
F. B. Dehn (communicated by Collins Radio Co.). Application date 20th June, 1946.

613 854.—Repeater system arranged to deal with two or more signals, which are travelling either in the same or in opposite directions.

The General Electric Co. Ltd. and A. S. Gladwin. Application date 21st January, 1946.

613 902.—Repeater systems for the two-way transmission of short-wave signals, and of the kind in which three frequency-changing stages are connected in cascade (divided from 613 854).

The General Electric Co. Ltd. and A. S. Gladwin. Application date 21st January, 1946.

614 005.—Thermo-electric device for measuring the level of power flowing through the coupling between a coaxial transmission line and a waveguide.

Sperry Gyroscope Co. Inc. Convention date (U.S.A.) 28th February, 1945.

614 066.—Frequency-modulating system in which the oscillator is stabilized by a transmission-line feedback-connection longer than one wavelength of the mean carrier frequency.

Standard Telephones and Cables Ltd. (assignees of G. T. Roden). Convention date (U.S.A.) 15th September, 1945.

614 243.—Radio transmitter in which the amplitude of a carrier wave is varied by the so-called phase-swing method of applying the signal to the grids of a pair of amplifying valves.

Marconi's W. T. Co. Ltd. and T. H. Price. Application date 17th April, 1946.

614 729.—Relay device for preventing the blocking-out click from being heard in a two-way radio communication system.

Philips Lamps Ltd. Convention date (Netherlands) 15th March, 1943.

615 073.—Frequency-modulator, suitable for a mobile transmitter, in which signals applied to the screen grid of a pentode valve vary the carrier frequency through the so-called Miller effect.

The British Broadcasting Corporation and R. H. Hammans. Application date 22nd August, 1946.

615 216.—Flexible coupling for connecting two rigid lengths of waveguide, comprising a number of separate sheets with horn-shaped perforations which inter-engage concertina-wise.

Philco Radio and Television Corporation. Convention date (U.S.A.) 31st May, 1944.

616 004.—Two-way signalling system, in which frequency stability, conbined with a wide range of tuning, is ensured by the use of three local oscillators.

Marconi's W. T. Co. Ltd. (assignees of R. A. Varone). Convention date (U.S.A.) 4th August, 1945.

616 030.—Device for varying the attenuation, or the field orientation, of the energy travelling through a circular waveguide.

C. W. Miller and Metropolitan-Vickers Electrical Co. Ltd. Application date 21st August, 1946.

SIGNALLING SYSTEMS OF DISTINCTIVE TYPE

613 240.—Receiver installation for a multi-channel system of pulsed signalling, comprising gating and selecting valves for feeding the demodulator.

Standard Telephones and Cables Ltd. and C. G. Treadwell. Application date 12th June, 1946.

613 833.—Broadcasting system for ultra-short waves, wherein a number of separate transmitters radiate trains of pulses, each at the same amplitude, width and repetition-frequency, but each having a difierent mean phase position to any of the others.

Marconi's W. T. Co. Ltd. (assignees of C. W. Hansell. Convention date (U.S.A.) 4th August, 1943.

613 961.—System for the transmission of facsimile or like signals by means of trains of impulses, each preceded by a pilot or synchronizing pulse.

Sadir-Carpentier. Convention date (France) 31st May, 1945.

614 172.—Facsimile signalling system of the kind in which repeated trains of impulses represent specific built-up characters or symbols.

Standard Telephones and Cables Ltd. (assignees of N. H. Young, Jr.). Convention date (U.S.A.) 24th April, 1943.

614 805.—Time-modulation circuit for a multi-channel system of pulsed signalling.

The General Electric Co. Ltd. and M. M. Levy. Application date 31st July, 1946.

CONSTRUCTION OF ELECTRON-DISCHARGE DEVICES

614 313.—Construction and arrangements of the sensitive storage screen, in a two-gun cathode-ray tube, for improving the signal/noise ratio.

Marconi's W. T. Co. Ltd. (assignees of T. T. Eaton). Convention date (U.S.A.) 30th July, 1943.

620 859.—Cavity-resonator discharge device for increased power output having two radially-spaced resonator chambers and a field-free passage for the electrons passing to a collector.

Westinghouse Electric International Co. Convention date (U.S.A.) 26th June, 1942.

622 001.—Indirectly-heated cathode, the heater of which has two or more V portions, having longitudinal constrictions to separate one V from the next.

The M-O Valve Co. Ltd. and G. V. H. Freeman. Application date 10th March, 1947.

622 290.—Magnetron, an anode of which consists of segments parallel to the cathode axis, which segments form the capacitance of a cavity resonator.

"Patelhold" Patentverwertungs and Elektro-Holding A.G. Convention date (Switzerland) 12th September, 1945.

SUBSIDIARY APPARATUS AND MATERIALS

620 749.—Control switch (e.g., a time switch) for radio apparatus, in which the switch-operating winding is used as a smoothing inductance.

The General Electric Co. Ltd. and F. N. Garthwaite. Application date 24th August, 1945.

620 991.—Coaxial cable using interfitting spacers, each comprising a central partition with smaller and larger cylindrical parts on the two sides.

Compagnie Generale D'Electricité. Convention date (France) 9th April, 1946.

621 150.—Iron-dust core for enclosing toroidal coils, in which two core parts overlap along cylindrical surfaces.

M.V.G.B.D.M. de Montigny. Convention date (France) 15th December, 1943.

622 057.—Resonant circuit for u.h.f. including a concentrated capacitance with spiral electrodes one of which varies in width in a stepwise manner.

Philips Lamps Ltd. Convention date (Netherlands) 24th May, 1944.

622 823.—Signal attenuator of wide frequency range using electronic impedances.

Philco Corporation (assignees of M. E. Ames, Jr.). Convention date (U.S.A.) 30th December, 1944.